Deep Eutectic Solvent-Assisted Nitrogen, Chloride-Functionalized Carbon Quantum Dots: A Fluorescence Turn On-Off-On Approach for Detection of Mercury (II) and Glutathione in the Nanomolar Range

A Dissertation

Submitted in partial fulfilment of the

Requirements for the award of the Degree of

Master of Science

In

Chemistry

Submitted by

Shivam Khare

Registration No.: 302102016

Under the Supervision of

Dr. Banibrata Maity

Assistant Professor

School of Chemistry & Biochemistry

Thapar Institute of Engineering & Technology

Patiala-147004, Punjab, India

July 2023

DECLARATION

I, **Shivam Khare**, hereby declare that the work presented in this dissertation entitled "***Deep Eutectic Solvent-Assisted Nitrogen, Chloride-Functionalized Carbon Quantum Dots: A Fluorescence Turn On-Off-On Approach for Detection of Mercury (II) and Glutathione in the Nanomolar Range***" is my original work and was conducted under the guidance of **Dr. Banibrata Maity** at the **School of Chemistry & Biochemistry, Thapar Institute of Engineering & Technology, Patiala**, from **January 2023 to July 2023**. The matter presented in this dissertation has not previously been submitted to obtain any other degree or diploma in this or any other university or institute of learning. I hereby affirm that due recognition and proper acknowledgement have been accorded to the researchers whose works have been referenced in this dissertation.

Further, I declare that I have not intentionally copied any other person's work, paragraphs, text, data, results, etc., reported in journals, books, magazines, reports, dissertations, theses, etc. Furthermore, I have not included any such content in this dissertation and have not claimed it as my work in any citations.

Date: 26/07/2023 **Shivam Khare**

Place: TIET, Patiala **Registration No.:** 302102016

Dr. Banibrata Maity
Assistant Professor
School of Chemistry & Biochemistry
Thapar Institute of Engineering & Technology,
(Deemed to be University)
Patiala –147004 (India)

Mob: +91-7797833175
Email: banibrata.maity@thapar.edu
baniiitchem@gmail.com
URL: www.thapar.edu

CERTIFICATE

This is to certify that the dissertation entitled **"*Deep Eutectic Solvent-Assisted Nitrogen, Chloride-Functionalized Carbon Quantum Dots: A Fluorescence Turn On-Off-On Approach for Detection of Mercury (II) and Glutathione in the Nanomolar Range*"**, being submitted by **Shivam Khare (Registration No.: 302102016)** to the **School of Chemistry & Biochemistry, Thapar Institute of Engineering & Technology, Patiala**, in partial fulfilment of the requirements for the award of the degree of **Master of Science** in **Chemistry**, is an authentic record of research work carried out by him under my supervision and guidance.

The dissertation has met the standards and fulfilled the requirements of the rules and regulations relating to the nature of the degree. The contents embodied in the dissertation have not been submitted for the award of any other degree or diploma in this or any other university or institute of learning.

Date: 26/07/2023

Place: TIET, Patiala

Banibrata Maity

Signature

Dr. Banibrata Maity
Assistant Professor
School of Chemistry & Biochemistry
TIET, Patiala

TABLE OF CONTENTS

Page No.

ACKNOWLEDGEMENT **iii**

LIST OF TABLES **iv**

LIST OF FIGURES **v**

LIST OF SYMBOLS & ABBREVIATIONS **vi**

ABSTRACT **vii**

CHAPTER 1: INTRODUCTION **1-6**

1.1. Carbon Quantum Dots (CQDs): an overview 1

1.2. Methods for the Synthesis of CQDs 2

1.2.1. Top-down method 2

1.2.2. Bottom-up method 2

1.3. Surface Modification of CQDs 3

1.3.1. Surface Passivation and Functionalization 3

1.3.2. Heteroatoms Doping 4

1.4. Deep Eutectic Solvents (DESs): an overview 5

1.4.1. DESs as a Green Solvent 5

1.4.2. Preparation Methods of DESs 5

CHAPTER 2: LITERATURE REVIEW **7-11**

2.1. Recent developments in the synthesis and applications of CQDs 7-10

2.2. Research gaps 10

2.3. Objectives of the Dissertation 11

CHAPTER 3: MATERIALS AND METHODS **12-14**

3.1. Reagents and materials 12

3.2. Preparation of Deep Eutectic Solvent (DES) 12

3.3. Synthesis of N,Cl-CQDs 12

3.4. Instrumentations 13

3.5. Fluorescence quantum yield 14

3.6. Methodology for detection of Hg^{2+} and GSH 14

CHAPTER 4: RESULTS AND DISCUSSION 15-29

4.1. Synthesis of N,Cl-CQDs 15

4.2. Characterizations of N,Cl-CQDs 15-18

4.3. Optical properties of N,Cl-CQDs 19

4.4. Optical stability of N,Cl-CQDs 20

4.5. Selectivity towards Hg^{2+} 21

4.6. Detection of Hg^{2+} 22-23

4.7. Recovery of N,Cl-CQDs by GSH 24-26

4.7.1. Selectivity towards GSH 24

4.7.2. Detection of GSH 25

4.8. Plausible Sensing Mechanism 27-29

CONCLUSION 30

REFERENCES 31-40

ACKNOWLEDGEMENT

I am pleased to express my most profound gratitude to **Dr. Satnam Singh**, Professor and Head, SCBC, TIET, Patiala, for providing me with an opportunity to work on a dissertation.

I sincerely thank my supervisor **Dr. Banibrata Maity**, Assistant Professor, SCBC, TIET, Patiala, for his continuous support, guidance, encouragement, unsurpassed knowledge, generous help, insightful critique and discussions that resulted in the completion of this dissertation work.

I sincerely thank **Dr. Soumen Basu**, Professor, SCBC, TIET, Patiala, for facilitating me with the necessary lab requirements throughout my research.

I sincerely thank **Dr. Vijay Luxami**, Professor, SCBC, TIET, Patiala, for her kind permission for the lifetime measurements of my samples.

I sincerely thank **Dr. Mily Bhattacharya**, Assistant Professor, SCBC, TIET, Patiala, for providing me with the required facilities during my dissertation.

I extend my most profound gratitude to **all the faculty members and staff of the SCBC**, TIET, Patiala, for their continuous encouragement, help and support.

I am grateful to **Dr. Bhupendrakumar Chudasama**, Professor, SPMS, TIET, Patiala, for his kind permission for the zeta potential analysis of my samples.

I extend my special thanks to **Dr. Neeraj Sohal**, Project associate, SCBC, TIET, Patiala, and **Ms. Mandeep Kaur**, PhD Scholar, SCBC, TIET, Patiala, for their immense cooperation and timely help during the complete span of my dissertation work.

I sincerely thank **CRF, IIT Ropar** for the XPS analysis of my samples.

I am grateful to **CIL, Panjab University**, Chandigarh, for the TEM analysis of my samples.

I sincerely thank **Research facility of SPMS, TIET Patiala** for the XRD analysis.

I sincerely thank **Research facility of TIET-VT CEEMS** for the FTIR analysis.

My heartfelt thanks to all my seniors, friends and classmates for their help, cooperation and moral support.

My appreciation and gratitude towards my parents. My parents have been an eternal source of inspiration and are my foundation. Whatever I am and intend to be because of my parent's unfailing love, affection and encouragement.

Date: 26/07/2023 **Shivam Khare**

LIST OF TABLES

Page No.

Table 2.1: A summary of CQDs prepared from different precursors. 9-10

Table 4.1: Comparative study of different sensing systems for detecting Hg^{2+} ions. 24

Table 4.2: Comparative study of different sensing systems for the detection of GSH. 26

Table 4.3: Photophysical parameters of N,Cl-CQDs with Hg^{2+} ions and GSH. 29

LIST OF FIGURES

Page No.

Figure 1.1:	Sources of Biomass-based precursors.	2
Figure 1.2:	Top-down & bottom-up synthesis method.	3
Figure 1.3:	Different types of DESs.	6
Figure 3.1:	Schematic synthesis diagram of N,Cl-CQDs.	13
Figure 4.1:	Reaction time optimization of N,Cl-CQDs.	15
Figure 4.2:	TEM images and Particle size distribution of N,Cl-CQDs.	16
Figure 4.3:	EDS spectra of N,Cl-CQDs.	16
Figure 4.4:	XRD and FTIR spectra of N,Cl-CQDs.	17
Figure 4.5:	XPS survey spectra of N,Cl-CQDs.	18
Figure 4.6:	XPS graph of C 1s, N 1s, O 1s and, Cl 2p of N,Cl-CQDs.	18
Figure 4.7:	UV-vis absorbance spectra of N,Cl-CQDs.	19
Figure 4.8:	PL excitation & emission spectra of N,Cl-CQDs.	20
Figure 4.9:	Stability of N,Cl-CQDs at different pH values, UV irradiation time, Storage time and Concentration of NaCl.	21
Figure 4.10:	Selectivity and interference studies of N,Cl-CQDs for Hg^{2+} detection.	22
Figure 4.11:	Effect of different concentrations of Hg^{2+} on PL intensity of N,Cl-CQDs, Stern-Volmer plot between F_0/F & different concentrations of Hg^{2+} ions.	23
Figure 4.12:	Linear correlation between F_0-F/F_0 & different concentrations of Hg^{2+} (0 to 0.85 μM) with inset image of concentrations of Hg^{2+} (0 to 0.35).	23
Figure 4.13:	Selectivity and interference studies of N,Cl-CQDs + Hg^{2+} system for GSH detection.	25
Figure 4.14:	Effect of different concentrations of GSH on the PL intensity of N,Cl-CQDs + Hg^{2+} sensing system and Linear correlation between F_0-F/F_0 & different concentrations of GSH (0 to 0.60 μM).	26
Figure 4.15:	UV absorbance spectra of N,Cl-CQDs without Hg^{2+}, and with Hg^{2+} & Lifetime studies of N,Cl-CQDs in the presence of Hg^{2+} & GSH.	28
Figure 4.16:	Zeta potential values of N,Cl-CQDs in the presence of Hg^{2+} and GSH.	28
Figure 4.17:	Plausible turn "On-Off-On" mechanism of N,Cl-CQDs.	28

LIST OF SYMBOLS & ABBREVIATIONS

nM: Nanomolar

µM: Micromolar

mM: Millimolar

M: Molar

nm: nanometer

eV: electronvolt

mV: millivolt

pH: Potential of Hydrogen

°C: Degree Celsius

UV: Ultraviolet

Vis: Visible

PL: Photoluminescence

QY: Quantum yield

CQDs: Carbon Quantum Dots

DESs: Deep Eutectic Solvents

HBD: Hydrogen bond donor

HBA: Hydrogen bond acceptor

HSAB: Hard and soft acids and bases

HOMO: Highest occupied molecular orbital

LUMO: Lowest unoccupied molecular orbital

TCSPC: Time-correlated single-photon counting

N,Cl-CQDs: Nitrogen & Chloride co-doped carbon quantum dots

ABSTRACT

In this work, we present a novel technique for the synthesis of Nitrogen & Chloride co-doped carbon quantum dots (N,Cl-CQDs) using a Choline chloride-urea based green deep eutectic solvent (DES) via a Microwave synthesis approach. Wheatgrass *(Triticum aestivum)* was used as a carbon source. DES played a significant role in the multi-heteroatom doping of N and Cl in respective CQDs, which XPS, FTIR, and XRD analysis confirmed. The TEM images show the spherical shape of N,Cl-CQDs with a median particle diameter of 1.75 nm, ranging from 0.5 to 4.0 nm. The N,Cl-CQDs obtained a high quantum yield (QY), i.e. 36%, compared to un-doped CQDs, which were synthesized in an aqueous medium (QY 15%). The prepared N,Cl-CQDs showed significant properties such as excellent photostability, favourable water solubility, and high optical stability. Furthermore, Hg^{2+} ions were detected using N,Cl-CQDs (turn-off) with a LOD value of 39 nM in a range of 0 to 0.35 µM, achieved by the dynamic quenching mechanism. Different photophysical parameters were calculated to confirm the fluorescence quenching mechanism, including average lifetime values, fluorescence quantum yield, zeta potential, radiative rate constants (kr), and non-radiative rate constants (knr). The current sensing system possesses an appealing characteristic of functioning as a "turn-on" sensor for GSH detection with a LOD value of 43 nM in a dynamic range of 0 to 0.60 µM. The N,Cl-CQDs prepared in this study exhibited a reduced detection limit and a broad linear range by an easy, environmentally friendly, and rapid method for detecting GSH and Hg^{2+} ions.

CHAPTER 1

1. INTRODUCTION

1.1. Carbon Quantum Dots (CQDs): an overview

CQDs are a new class of zero-dimensional photo-luminescent nanoparticles with a spherical shape and particle size of less than 10 nm, discovered in 2004 by Xu *et al.*[1] The core of CQDs is a fusion of sp^2-hybridized graphitic carbon or sheets of graphene oxide combined with diamond-like carbon fragments, which are sp^3-hybridized.[2] Recently, CQDs have gained significant attention due to their excellent optical properties, photostability, high quantum yield, low toxicity, water solubility, favourable biocompatibility, and good selectivity and sensitivity towards target analytes with tunable fluorescence excitation and emission with significant stokes shift.[3] However, the mechanism that results in fluorescence is quite complicated. Surface defects, quantum confinement, emissive traps, and aromatic structure are just some of the current hypotheses put forward to explain it.[4] CQDs have vast applications in cell imaging,[5] drug delivery,[6] chemical sensing,[7] electrochemistry,[8] photocatalysis,[9] energy conversion, and storage.[10] The CQDs can be synthesized from various carbon sources like chemical-based precursors (citric acid,[11] glycerol,[12] graphene oxide,[13] chitosan[14]) and natural precursors (biomass and bio-waste). The chemical precursors have limitations like cytotoxicity, harsh reaction conditions, post-surface passivation, low yield, and cost of the source.[15] Therefore, bio-waste and biomass-based precursors (Figure 1.1) gained much attention among researchers due to their easy availability, low cost, biocompatibility, biodegradability, high carbon content, and stable optical properties.[16] Various plant species are employed as renewable carbon sources to synthesize CQDs. Different parts of plants, like stems, flowers, leaves, fruits, fruit juice, bark, kernel, stalk, shells, and peels, are primarily used to synthesize CQDs.[17] Researchers have reported CQDs from pea-nut shells,[18] rice husk,[19] orange pomace,[20] mango leaves,[21] tea residues,[22] banana peels,[23] neem leaves,[24] and other biomass sources. Contrary to the CQDs synthesized from artificial sources, which require various chemical reagents for the surface functionalization of heteroatoms on CQDs, biomass containing heteroatoms is the best source for synthesizing CQDs. Besides this, Nowadays, Deep eutectic solvents (DESs) are gaining much attention for synthesizing doped CQDs because DESs have abundant elements for the surface functionalization and doping of CQDs and are non-toxic green solvents. The CQDs are mainly synthesized via “top-down” and “bottom-up” approaches.

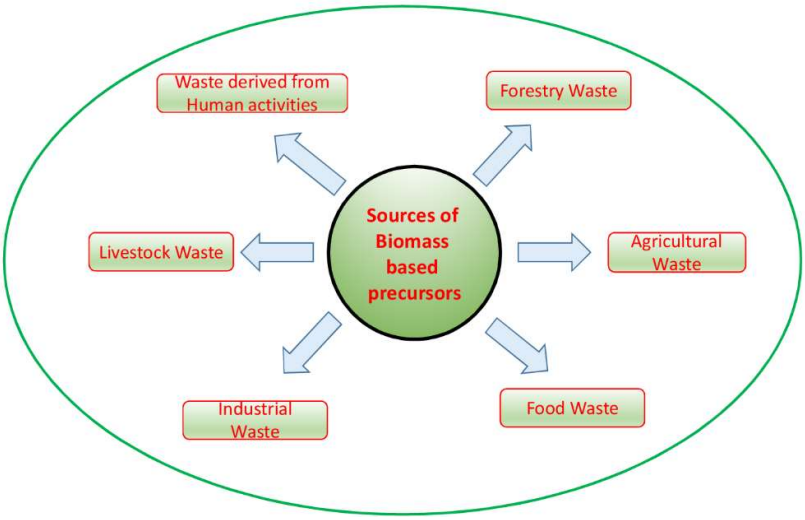

Figure 1.1: Sources of Biomass-based precursors.

1.2. Methods for the Synthesis of CQDs

1.2.1. Top-down method

The top-down approach involves converting bulky carbonaceous materials (graphite, carbon nanotube, large-size graphene) into nanoscale CQDs (Figure 1.2).[25] The top-down method includes arc discharge, laser ablation, and electrochemical oxidation.[26,27] Top-down approaches typically involve harsh reaction procedures (such as strong acid and arc discharge), prolonged reaction times and expensive equipment, which severely restrict the practical application of CQDs.[28]

1.2.2. Bottom-up method

The bottom-up approach involves the conversion of small molecules into nanoscale CQDs via the carbonization of natural precursors under thermal, hydrothermal, solvothermal, pyrolysis, ultra-sonication and microwave methods (Figure 1.2).[29] The bottom-up technique is generally advantageous for introducing heteroatom doping into the synthesis process since it has a high yield. Also, this method is easy, cost-effective and requires minimum equipment.[30] Thus, the synthesis of CQDs has frequently adopted this approach. In the bottom-up approach, the most widely used methods are hydrothermal and microwave synthesis of CQDS. A hydrothermal method is a green, inexpensive, non-toxic one-pot synthesis method which involves heating of reaction mixture in an aqueous medium from 2 hours to 12 hours, usually at a temperature above 100°C and pressure 1 bar in a closed vessel.[31] Hydrothermal-based reactions generally take a longer time compared to microwave synthesis. The microwave synthesis method is a

green, inexpensive, cleaner and faster way than the hydrothermal synthesis method. It involves homogenous heating of the reaction mixture and takes only 0.2 to 120 minutes to complete the reaction process. Microwave irradiation targets the depth of a molecule and performs uniform heating instead of conduction and convection-based heating.[32]

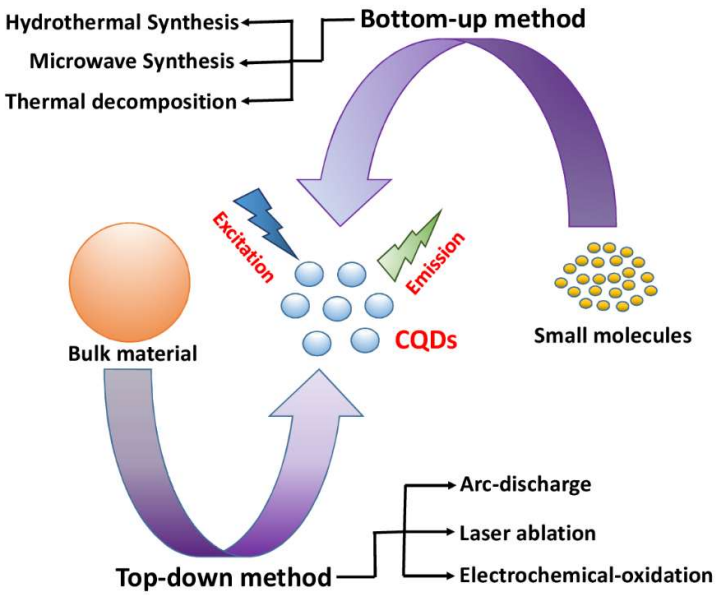

Figure 1.2: Top-down & bottom-up synthesis method.

1.3. Surface Modification of CQDs

1.3.1. Surface Passivation and Functionalization

CQDs surfaces are sensitive to the environment and contaminants, and even minute amounts of contaminants can affect the properties of CQDs. To resolve this problem, surface passivation of CQDs is done to lessen the harm that surface contaminant causes to their optical properties. Surface passivation is often accomplished by creating a thin insulating layer, typically by attaching polymeric materials, such as oligomeric PEG and PEG1500N, to a CQDs surface that has undergone acid treatment.[33] Effective passivation of the surface can produce highly intensified CQDs. On the other hand, CQDs with unpassivated surfaces or naked surfaces may exhibit vibrant fluorescence, but they typically have poor quantum yields.[34] The insertion of functional groups onto the surface of the CQDs, such as amines, carbonyls, hydroxyls and sulfonates, has the potential to induce various defects on the surface of CQDs. These defects function as traps for excitation energy, resulting in significant fluctuations in fluorescence emissions. It is widespread for surface passivating agents to work as functionalizing agents,

changing CQDs physical and fluorescent characteristics. Therefore, further synthesis modification procedures are unnecessary.[35]

1.3.2. Heteroatoms Doping

The primary motivation for doping in CQDs is to develop a straightforward and efficient strategy that increases the number of active sites and improves the fundamental properties by utilizing lone pairs of electrons in the heteroatom. The dopants can enhance fluorescence by modifying the bandgap and introducing additional energy levels. These dopants can be either metallic or nonmetallic in nature. Dopants change the electron distribution of CQDs, which results in sp^2 hybridization in the core and sp^3 hybridization in the shell and also changes the surface structure. [36] The quantum yield can be enhanced by incorporating nonmetallic dopants, as they effectively reduce the energy gap between the nonbonding (n) orbital and π orbital of carbon. In contrast, the band structure is modulated by metallic dopants through their chelation with the functional groups present in the precursors during the process of carbonization.[37]

1.4. Deep Eutectic Solvents (DESs): an overview

DESs have garnered significant attention in the field of CQDs synthesis. The term "deep eutectic solvents" was initially introduced by Abbott *et al*. in 2003. In their study, they observed a significant reduction in the melting point of choline chloride and urea mixtures, exceeding temperature 100°C.[38] The synthesis process of CQDs can be affected by the choice of solvent, leading to variations in their surface and optical properties. The majority of synthesis techniques use solvents. The properties of the solvent have an impact on both the performance and morphology of the CQDs.[39] The discovery of ionic liquids was first documented by Walden in 1914.[40] An ionic liquid is composed of an organic cation and a large inorganic anion. In the past decade, these solvents were initially regarded as environmentally friendly options. However, contemporary understanding has revealed that many of these solvents exhibit volatility, flammability, and toxicity. ILs are also expensive, which limits their implementation in pilot applications.[41] On the other hand, DESs are green, biocompatible and, biodegradable solvents formed by hydrogen bonds interaction between a hydrogen bond acceptor (HBA) and a hydrogen bond donor (HBD) at a specific molar ratios and temperatures.[42] Both ionic liquids (ILs) and deep eutectic solvents (DESs) exhibit higher environmental sustainability than conventional solvents. The commonalities between ILs and DESs encompass a broad liquid temperature range, low volatility, high tunability, and the capacity to dissolve diverse substances. Both substances exhibit elevated levels of viscosity and density, which impose

limitations on their practical applicability.[41] The viscosity and density of substances are subject to variation based on their composition and temperature. The properties of DESs can be altered through the careful selection of initial compounds, molar ratio, and the inclusion of water as an additional component. A significant amount of water can lead to the decomposition of the DES.

1.4.1. DESs as a Green Solvent

DESs have dual applications as doping agents and green solvents.[43] The utilization of DESs offers several advantages over traditional organic solvents, including low volatility, low toxicity, biodegradability, biocompatibility, environment-friendly, enhanced solubility of substrates and reactants, and increased thermal stability.[44] Additionally, they can offer a greater variety of doping elements for use in CQDs. The impact of heteroatom doping on various properties of CQDs has been experimentally demonstrated. Specifically, heteroatom doping has been found to alter the fluorescence quantum yield, the d002 value (graphene layers spacing in CQDs), the electronic structure, the crystal structure, the energy gap between the LUMO and HOMO, as well as the surface functional groups present in CQDs. Various non-metal dopants like S, N, B, P, F, Cl, I, Te and Se, as well as metal dopants like Cu, Mn, Zn, Fe, Co, Ru and Ge, were employed in the fabrication of doped carbon dots CQDs. N is considered an exceptionally effective dopant among the range of non-metal elements.[45]

1.4.2. Preparation Methods of DESs

The first known DES is based on Choline-chloride (HBA) and Urea (HBD) and has received the most attention, followed by Choline chloride-Ethylene glycol and Choline chloride-Glycerol.[46] Subsequently, researchers have investigated additional combinations of HBA and HBD, specifically examining alternative salts such as ammoniums, phosphoniums,[47] and imidazolium.[48] But so far, the most famous DESs that have been made are those based on Choline-chloride (HBA). This is because Choline-chloride is inexpensive, safe, biocompatible and biodegradable. Choline chloride is an important ingredient that may be derived from biomass and is frequently recognized as a component of the Vitamin B complex.[48] Various HBD, including polysaccharides, renewable polyols, amines, amides, carboxylic acids and alcohols, have been mixed with Choline-chloride to form different types of DESs.[49] Figure 1.3 shows the different types of DESs prepared by mixing various HBA and HBD. Different methods have been used to prepare DESs in a repeatable manner. The 'Heating method' is the most popular of them, presumably because it is the easiest. Other techniques are less common than heating, and more study is needed to comprehend their potential fully. Abbott et al.

pioneered the Heating method in 2003. Mixing and stirring HBA and HBD at a specific temperature produces a clear, transparent, homogenous liquid. Depending on the components, heating temperatures range from 40°C to 110°C. DES preparation requires proper heating, temperature and stirring time. Insufficient heating temperature or processing time might cause crystal formation and system heterogeneity.[50]

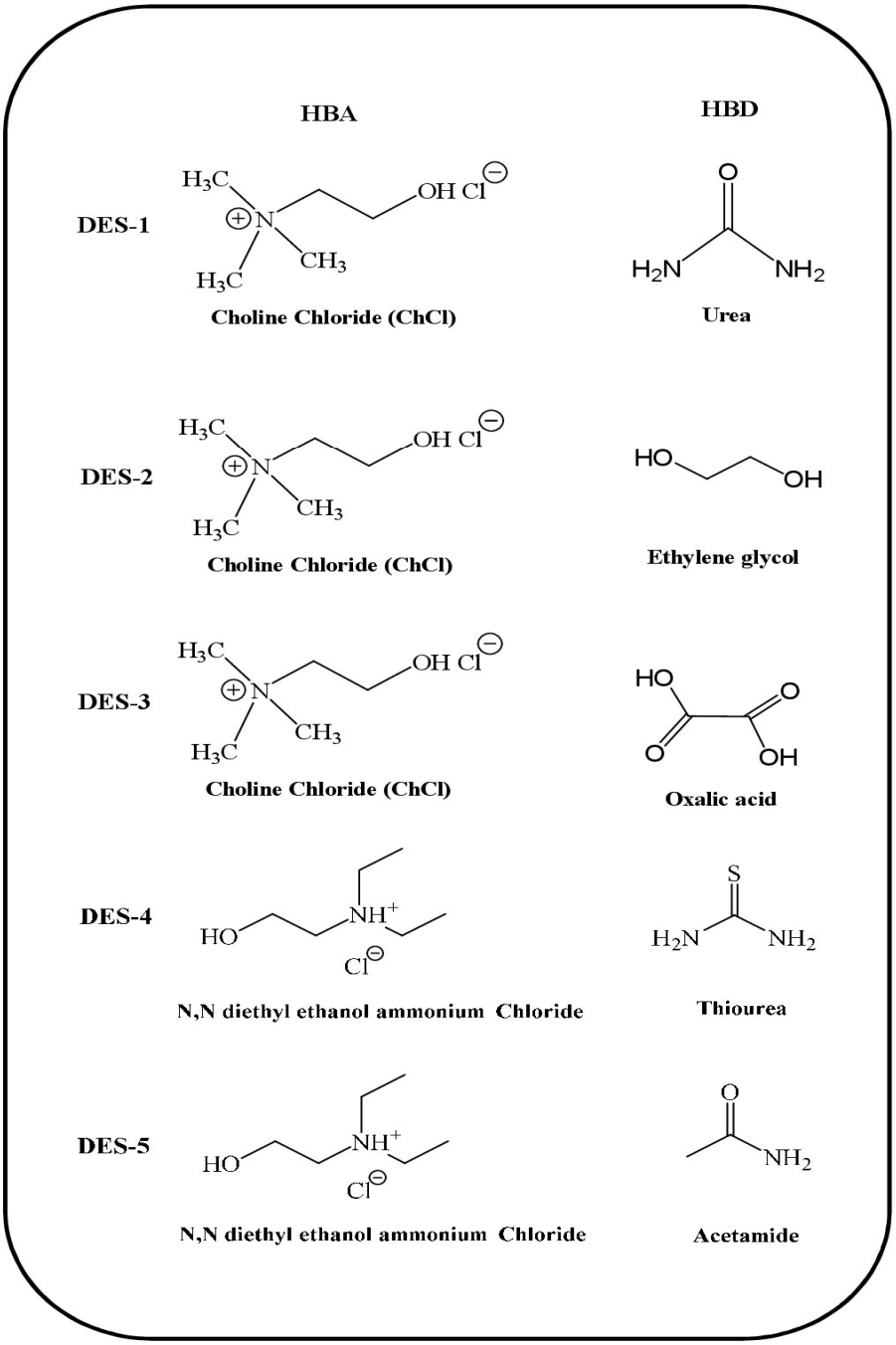

Figure 1.3: Different types of DESs.

CHAPTER 2

2. LITERATURE REVIEW

2.1. Recent developments in the synthesis and applications of CQDs

Sohal *et al.* (2023) synthesized two different types of inexpensive, simple, and eco-friendly Cdots, i.e. undoped carbon dots (u-Cdots) and nitrogen, sulphur co-doped carbon dots (N, S-Cdots), to detect Pb^{2+} ions through the rapid one-step process with high-temperature processing and no solvent. They have used citric acid and cysteine as a precursor for carbon, nitrogen and sulphur, respectively. The particle size of u-Cdots was measured to be 7.5 nm, while N, S-Cdots were estimated to be 1.8 nm. Dynamic quenching and aggregation-induced emission enhancement (AIEE) were responsible for Pb^{2+} detection. The LOD for the fabricated u-Cdots and N, S-Cdots sensing systems was 30 nM & 7 nM, respectively.[51]

Kundu *et al.* (2023) reported green microwave synthesis of CQDs from orange pomace. The synthesized CQDs were measured to have a median diameter of 7.5 nm. The fluorescent quantum yield of these synthesized CQDs was exceptionally high at 54.26%, and they also exhibited good photo-stability and water solubility. The synthesized CQDs revealed encouraging findings in detecting 4-NP (4-nitrophenol) and Cr^{+6} ions. CQDs were sensitive to 4-NP and Cr^{+6} with LOD values of 14 nM and 56.6 nM, respectively. Lifetime measurements (TCSPC) revealed a decrease in fluorescence intensity as the concentration of the quencher increased, which was explained by the inner filter effect.[20]

Liu *et al.* (2021) synthesized N, Cl-doped carbon dots (N, Cl-CDs) using green precursors derived from stems of *Impatiens balsamina L* in a DES via hydrothermal method. DES were prepared using Choline-chloride and acetamide. Doping N and Cl elements into the CDs using deep eutectic solvents (DES) resulted in exceptional sensitivity to and selectivity for Gram-positive bacteria and enhanced quantum yield. The typical size distribution of N, Cl-CDs ranged across 2 and 4.5 nm and had remarkable disparity and homogeneity. N, Cl-CDs also showed minimal cytotoxicity and excellent cell imaging capabilities in both normal cells and cancer cells. Furthermore, their sensors were capable of functioning as a florescent detector for the identification of ClO^- ion, exhibiting a detection range spanning from 100 nM to 40 µM and a LOD value as low as 30 nM.[52]

Pajewska-Szmyt *et al*. (2020) synthesized Nitrogen-doped CDs using citric acid and melamine via the hydrothermal method. The reported quantum yield was 44%. The highest excitation and

emission wavelength were recorded at 352 and 427 nm, respectively. The CDs were sensitive toward detecting Hg^{2+} ions through a turn-off sensing mechanism. The LOD achieved as low as 0.44 μM, within a dynamic range from 2 to 14 μM. Interestingly, for the first time, human milk was used in the real sample analysis to test the viability of CDs.[53]

Wang *et al.* (2022). They used deep eutectic solvent (DES) as a green solvent and doping agent to prepare Nitrogen & Sulphur doped CDs (N, S-CDs). They followed an ionothermal synthesis procedure and used cellulose as a carbon precursor. DES was prepared using sulfamic acid and urea. Cu^{2+} and GSH were detected sensitively using the reported CDs as an on-off fluorescence sensor. The fluorescent probe detects Cu^{2+} at 23.4 nM. GSH also stabilizes the Cu^{2+}-GSH complex, restoring CD fluorescence. Thus, the CDs-Cu^{2+} combination was an additional sensor with a 5.98 μM detection range. The reported quantum yield was 7.17%.[54]

Yin *et al.* (2021). They investigated the fabrication of N, Cl co-doped carbon dots (N, Cl-CDs) using a straightforward hydrothermal method, utilizing deep eutectic solvent (DES) with a quantum yield of 14%. The N, Cl-CDs were used for selective and sensitive detection of morphine in food samples. The intensity of carbon dots exhibited a linear increase when morphine was added within the range of 0.15 to 280.25 μg mL^{-1}. Additionally, the LOD was determined to be 46.5 ng ML^{-1}.[55]

Nazari *et al.* (2023) investigated CDs synthesize from ten choline-chloride based deep eutectic solvents, prepared via microwave synthesis approach. Glucose has been used as a carbon source precursor. The quantum yield of developed CDs in Choline chloride-urea, Choline chloride-thiourea, and Choline chloride-glycerol DESs were 41.3%, 35.5%, and 38.7%, respectively. Results indicated that the characteristics of CDs and doping were significantly influenced by the chemical structure of DESs hydrogen bond donors (HBD). As the carbon chain length of H-bond donors increases, its capacity to form hydrogen bonds and act as a hydrogen donor in DESs decreases. CDs with a higher quantum yield are generated from DESs with a shorter carbon chain and a greater abundance of -NH2 and -OH. N, Cl-doped CDs detected Atorvastatin with a LOD value of 0.8 nM, N, S-doped CDs were used to detect Fe^{3+}/Naproxen (LOD 25 nM), N-doped CDs (Choline chloride-acetamide) were used to detect Fe^{3+}/Cetirizine with LOD value of 10 nM and other N-doped CDs (Choline chloride-glycerol) were used to detect Co^{2+}/ Enrofloxacin with LOD value of 62 nM.[56]

Huang *et al.* (2022) synthesized tea derived carbon dots (CDs) using Choline chloride/urea based DES via a one-pot hydrothermal method. They have optimized molar ratios (1:1, 1:2,

and 1:3) of Choline chloride/urea and found that highest quantum yield of CDs were obtained using 1:2 mole ratio of DES. The prepared CDs exhibited sensitivity towards detection of Cd^{2+} with LOD value of 2.14 µg/mL in a linear range of 0–20 µg/mL.[57]

Table 2.1: A summary of CQDs prepared from different precursors.

Precursor	Synthesis Method	Target	LOD	Reference
Coriander leaves	Hydrothermal	Fe^{3+}	0.40 µM	[58]
Peanut shells	Pyrolysis	Cu^{2+}	4.8 µM	[59]
Lemon peel	Hydrothermal	Cr^{6+}	73 nM	[60]
Osmium sanctum	Hydrothermal	Pb^{2+}	0.59 nM	[61]
Tobacco	Hydrothermal	Tetracycline	5.18 nM	[62]
Alfalfa and garlic	Hydrothermal	Biothiols	86 nM	[63]
Tender coconut water	Microwave	Thiamine	280 nM	[64]
Sewage sludge	Microwave	Para-Nitrophenol	0.06 µM	[65]
Jackfruit seeds	Microwave	Au^{3+}	239 nM	[66]
Saffron	Hydrothermal	Prilocaine	1.8 nM	[67]
Wool	Microwave	Glyphosphate	12 ng/mL	[68]

Sophora flavescens	Hydrothermal (DES-assisted)	Myricetin	10 nM	[69]
Chamomile	Solvothermal (DES-assisted)	Tartrazine and Fe^{3+}	40 nM and 119 nM	[70]
Cellulose	Ionothermal (DES-assisted)	Cu^{2+} and Glutathione	23.4 nM and 5.98 μM	[71]
Glucose	Microwave (DES-assisted)	Citrizine	15 nM	[72]

2.2. Research gaps

Based on a thorough review of the relevant literature and the contextual information provided above, the following research gaps have been identified:

- The majority of CQDs reported in the literature go through hetero-atom doping to improve their fluorescence properties by using toxic solvents and chemical reagents, which is not an eco-friendly approach. This limitation can be overcome by using green DESs to synthesize CQDs.
- Minimal literature reported on the photophysics of DESs-derived CQDs and their sensing application. Therefore, the photophysical study of DESs-derived CQDs is done to explore their potential application in heavy metal ions sensing and biomolecule sensing.
- To the best of our knowledge, there is currently no literature available that has explored the potential of DESs derived CQDs using biomass-based precursor for the dual-analyte sensing of the Hg^{2+} and GSH via a turn “On-Off-On” sensing mechanism.

2.3. Objectives of the Dissertation

This research aims to synthesize multi-heteroatom co-doped DES-assisted CQDs with significantly high fluorescence quantum yield using biomass-based precursors via a facile, green, one-step Microwave synthesis approach. To explore the sensing application of DES-assisted CQDs for detecting heavy metal ions and biomolecules via a turn “On-Off-On” mechanism. Furthermore, the primary emphasis lies in detecting analytes within the nanomolar range using the synthesized N,Cl-CQDs, proving its potential as a strong contender in the sensing field. Detailed photophysical parameters were calculated to confirm plausible sensing mechanism of dual-analytes.

CHAPTER 3

3. MATERIALS AND METHODS

3.1. Reagents and materials

Choline chloride (ChCl) and Urea were purchased from Loba Chemie, India, to prepare deep eutectic solvent and used without further purification. Biomass-based precursor "*Triticum aestivum"* (Wheatgrass) has been used as a carbon source. The wheatgrass saplings were obtained from local farmers of the Patiala, India region. NaOH, HCl (for pH optimization), NaCl (for ionic strength optimization) and Quinine sulfate (for quantum yield determination) were obtained from Loba Chemie, India. All the metal salts ($HgCl_2$, $FeCl_3$, KCl, $MgCl_2$, $FeCl_2$, $NiCl_2$, $Cr(NO_3)_3$, $MnCl_2$, $Pb(NO_3)_2$, $BaCl_2$, $CoCl_2$, NH_4Cl, $CuCl_2$) used in this work were obtained from Loba Chemie, India. All the biomolecules, i.e. Glucose, Dopamine, Cysteine, Arginine, Methionine, Leucine, Histidine, Asparagine, Glutathione, Valine, Glutamic Acid, Glutamine, Lysine, Alanine, Aspartic Acid, Isoleucine, and Threonine were obtained from HiMedia Laboratories. Ultra-pure deionized (DI) water was used to prepare stock solutions for further investigation.

3.2. Preparation of Deep Eutectic Solvent (DES)

Choline chloride (HBA) and Urea (HBD) were used to prepare DES by the following procedure: 13.9 g of choline chloride and 12.8 g of urea with a molar ratio of 1:2 were taken in a 100 ml beaker and heated at 80°C with continuous stirring for 30 minutes until a transparent homogenous liquid was obtained.[57,73] This green solvent was later stored in a desiccator.

3.3. Synthesis of N,Cl-CQDs

N,Cl-CQDs were synthesized using the Microwave synthesis method. In brief, wheatgrass saplings were put in a grinder/mixture, and pure juice was obtained. Next, 4 ml of wheatgrass juice and 2 ml of DES were taken in a reaction vial and kept for heating with continuous stirring at 150°C for 40 minutes in a Microwave synthesizer.[20] The brown colour liquid was obtained and transferred in a falcon tube for centrifugation at 8000 rpm for 20 minutes at room temperature to remove large-size particles. The supernatant liquid was obtained and further filtered using a 0.2 µm membrane filter, resulting in the formation of Brown-coloured N,Cl-CQDs. Figure 3.1 shows the detailed schematic diagram of N,Cl-CQDs synthesis.

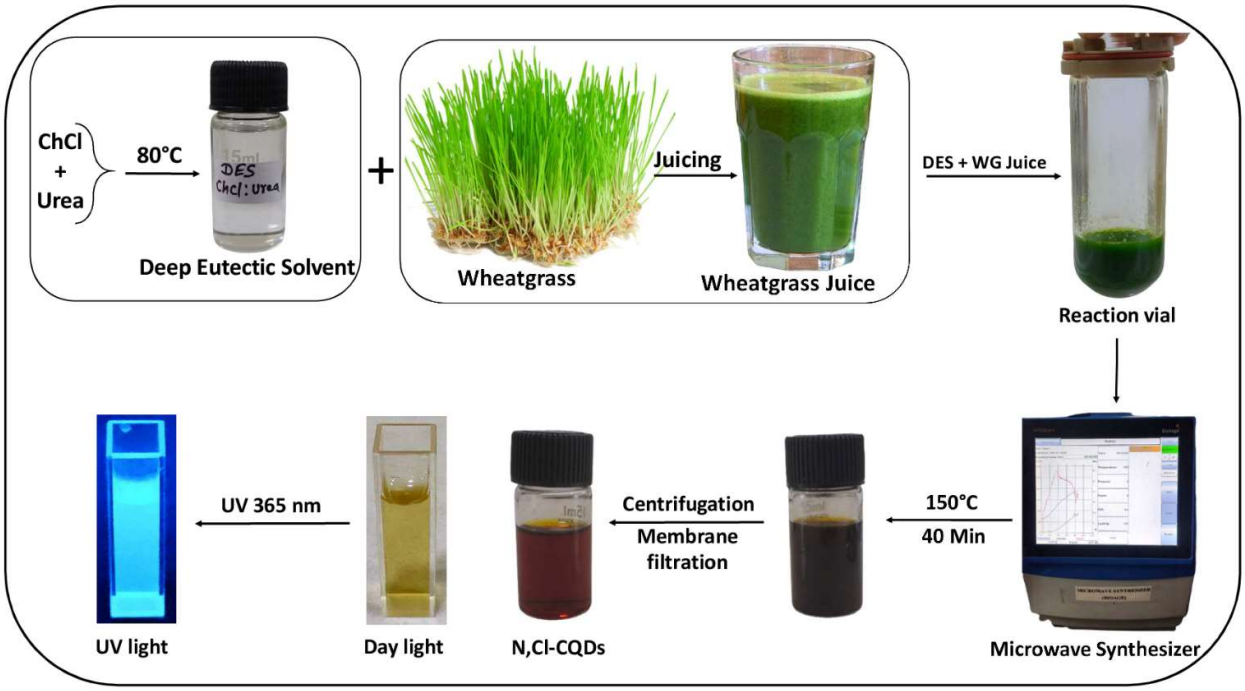

Figure 3.1: Schematic synthesis diagram of N,Cl-CQDs.

3.4. Instrumentations

Biotage Initiator+ Microwave synthesizer was used to prepare N,Cl-CQDs. Several spectroscopic techniques were used to characterize the synthesized N,Cl-CQDs. The UV-vis absorption spectrum was measured using a UV-vis spectrophotometer manufactured by Shimadzu Japan (model UV-2600). The PL emission spectrum was recorded on a Shimadzu spectrofluorometer (model RF-6000). Transmission electron microscopy (TEM) and Energy-dispersive X-ray spectroscopy (EDS) were carried out using the JEOL JEM 2100 plus instrument (JEOL USA), which determined the N,Cl-CQDs morphology, size, and shape. The crystal structure of N,Cl-CQDs was determined using an X-ray diffractometer (XRD) Model: SmartLab SE (Rigaku, Japan). Time-resolved fluorescence investigations were conducted using a Time-correlated single-photon counting (TCSPC) spectrometer, specifically the Horiba Jobin Yvon IBH model (Horiba, Japan). The fluorescence lifetime measurements were carried out with an excitation laser emitting at 450 nm. The Fourier-transform infrared spectrophotometer (FTIR, Shimadzu IRTracer-100) was used to investigate the functional groups. The XPS survey spectra were recorded using a Thermo Fisher Scientific (USA) X-ray photoelectron spectrometer (Model: Escalab Xi+). A Brookhaven 90 plus zeta potential analyser was used to measure the zeta potential. Centrifugation was performed using a Thermo Fisher Scientific SL 8R centrifuge instrument.

3.5. Fluorescence quantum yield

A reference method was used to calculate the quantum yield (QY) of N,Cl-CQDs at an excitation wavelength of 350 nm. The substance chosen for reference is quinine sulfate (dissolved in 0.1 M H_2SO_4 solution, QY = 0.54).[74] The quantum yield was calculated using the equation (1):

$$\phi_S = \phi_R \times \frac{A_S}{A_R} \times \frac{(Abs)_R}{(Abs)_S} \times \frac{\eta_S^2}{\eta_R^2} \quad (1)$$

The subscripts S and R in the equation represent the sample (N,Cl-CQDs) and reference (Quinine sulfate). ϕ_S Represents the QY of the sample, ϕ_R depicts the QY of reference, and A_S and A_R is the PL emission area of the sample and reference, respectively. "Abs" indicates absorbance, and "η" shows the refractive index.

3.6. Methodology for detection of Hg^{2+} and GSH

50 µL of N,Cl-CQDs dissolved in 2 mL of DI water has been taken in a cuvette for all the PL emission measurements. 1 mM stock solutions of all the metal ions and biomolecules have been prepared for selectivity studies. Further, sensitivity studies of Hg^{2+} were done using a 1 µM stock solution of Hg^{2+}, with different concentrations of Hg^{2+} ranging from 0.05 µM to 0.85 µM added to a cuvette containing 50 µL of N, Cl-CQDs dissolved in 2 mL DI water. Similarly, for GSH sensitivity studies, 1 µM stock solution is used with a dynamic range of 0.1 µM to 5.5 µM.

CHAPTER 4

4. RESULTS AND DISCUSSION

4.1. Synthesis of N,Cl-CQDs

Nitrogen (N) & Chloride (Cl) co-doped carbon quantum dots (N,Cl-CQDs) were prepared through a Microwave synthesis approach using *Triticum aestivum* (Wheatgrass) for the first time. Wheatgrass is the young grass of the wheat plant *Triticum aestivum.* DES is used as a green solvent and doping agent for doping heteroatoms (N, Cl) in respective CQDs. The following were the most optimal reaction circumstances: 2 mL of DES as the green solvent, 4 mL of pure wheatgrass juice as a carbon source, 150°C as the optimum reaction temperature, and 40 minutes as the reaction time in a microwave (Figure 4.1). The QY of prepared N,Cl-CQDs obtained was 36%, and the QY of N,Cl-CQDs increased substantially compared to CQDs prepared using water as a solvent (QY was 15%) which employs that heteroatoms doping in the CQDs structure enhanced the CQDs fluorescence capabilities.

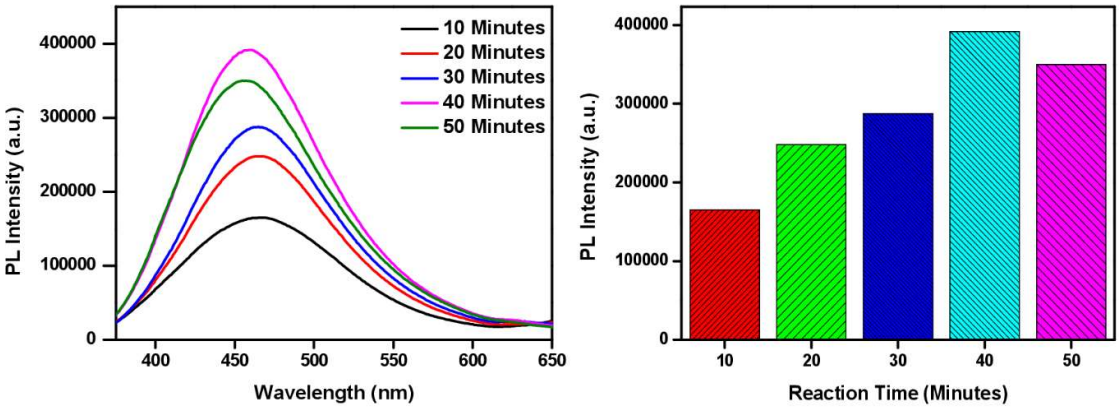

Figure 4.1: Reaction time optimization of N,Cl-CQDs.

4.2. Characterizations of N,Cl-CQDs

Transmission electron Microscopy (TEM) images of synthesized N,Cl-CQDs (Figure 4.2a,b) revealed that the prepared N,Cl-CQDs were spherical in shape with good disparity and uniformity. The average size distribution was in the range of 0.5 to 4.0 nm (Figure 4.2c), with an estimated mean particle size of 1.75 nm. Furthermore, The Energy-dispersive X-ray spectroscopy (EDS) spectra of N,Cl-CQDs shown in Figure 4.3 indicate the presence of C, N, O, and Cl elements which confirm the successful incorporation of N and Cl atoms in CQDs;

the percentage of elements present summarizes in the inset table of EDS spectra The peak of Cu is due to the presence of copper in the TEM grid; the statistics from EDS spectra showed that N,Cl-CQDs have a carbonaceous character, which is reflected by the increased percentage of carbon.

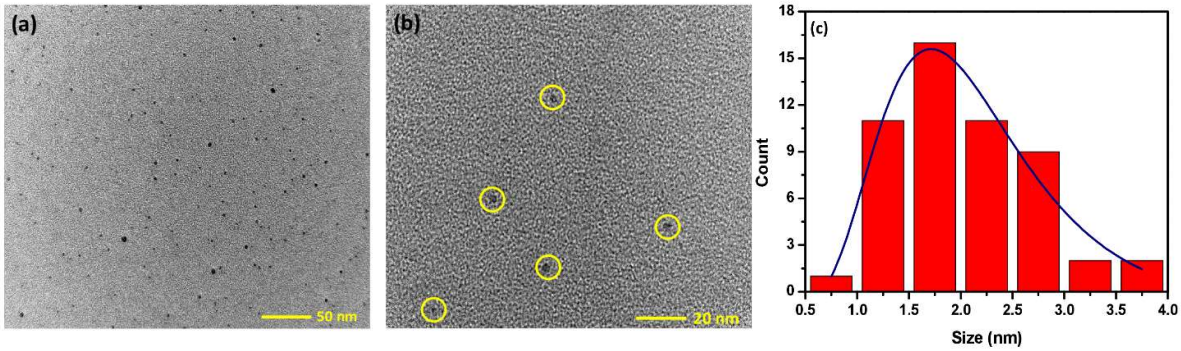

Figure 4.2: (a) and (b) shows TEM images of N,Cl-CQDs, (c) Particle size distribution of N,Cl-CQDs.

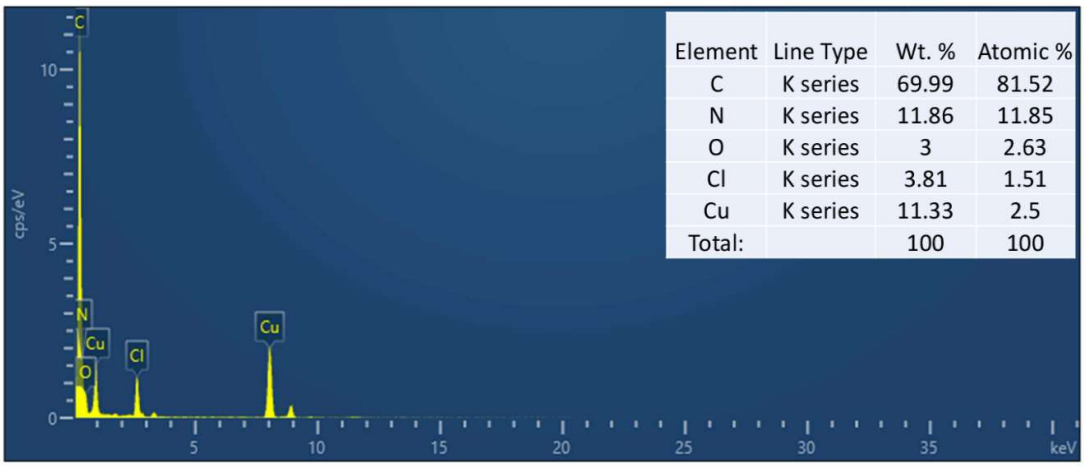

Element	Line Type	Wt. %	Atomic %
C	K series	69.99	81.52
N	K series	11.86	11.85
O	K series	3	2.63
Cl	K series	3.81	1.51
Cu	K series	11.33	2.5
Total:		100	100

Figure 4.3: EDS spectra of N,Cl-CQDs.

The X-ray diffraction (XRD) spectra in Figure 4.4a depict a broad, amorphous peak at 2θ = 24.1° corresponding to the (002) lattice spacing of the graphitic carbon plane present in N,Cl-CQDs structure.[75,76] The TEM, EDS data, and XRD results provide conclusive evidence that N,Cl-CQDs were successfully synthesized. Further characterization was done using Fourier-transform infrared spectroscopy (FT-IR) and X-ray photoelectron spectroscopy (XPS) to confirm the successful doping of N and Cl atoms. Synthesized N,Cl-CQDs were analyzed with an FT-IR spectrophotometer to gain insight into functional groups. Figure 4.4b reveals that the most substantial peaks at 3340, 3210, and 2980 cm^{-1} correspond to -O-H, -N-H and -C-H stretching vibrations. The absorptions peak at 1625 cm^{-1} was attributed to the C=C bond, and the distinctive absorption peak at 1461 cm^{-1} was most likely responsible for the C-N bond

vibrations.[77] Additionally, peaks at 1085 and 1160 cm^{-1} confirm the C-O stretching vibrations.[78]

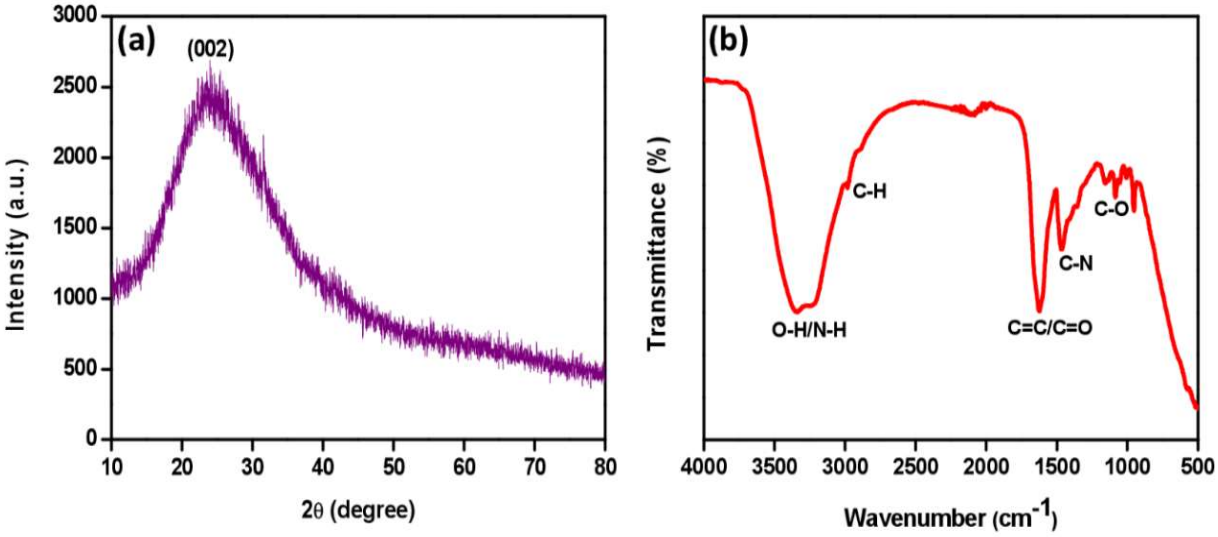

Figure 4.4: (a) XRD spectra of N,Cl-CQDs, (b) FTIR spectra of N,Cl-CQDs.

XPS was used to study the elemental composition of the N,Cl-CQDs. The survey spectra of XPS (Figure 4.5) represent four distinctive peaks for C 1s (284.9 eV), N 1s (399.8 eV), O 1s (531.9 eV), and Cl 2p (197.2 eV). The elemental analysis revealed the composition of C (63.08%), N (17.28%), O (17.06%), and Cl (2.58%). This finding elucidated the N and Cl doping on the surface of CQDs. Furthermore, the detailed C 1s spectrum indicate three significant peaks at 283.3, 284.7, and 286.8 eV, attributed to C-C/C=C, C-N, and C-O, respectively (Figure 4.6a). Similarly, the N 1s spectrum indicates two peaks at 398.7 and 401.3 eV, corresponding to the C-N and N-H, respectively (Figure 4.6b). The O 1s spectrum exhibited two peaks at 530.6 and 531.6 eV, corresponding to the O-H and C=O, respectively (Figure 4.6c). Two prominent peaks at 196.9 and 198.5 eV in the Cl 2p spectrum attributed to C-Cl and N-Cl, respectively (Figure 4.6d).[79,80,81]

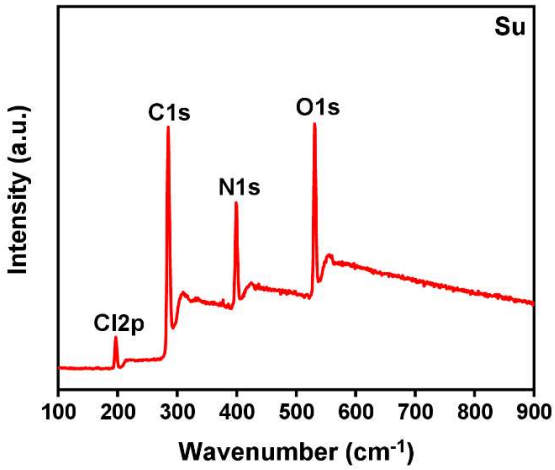

Figure 4.5: XPS survey spectra of N,Cl-CQDs.

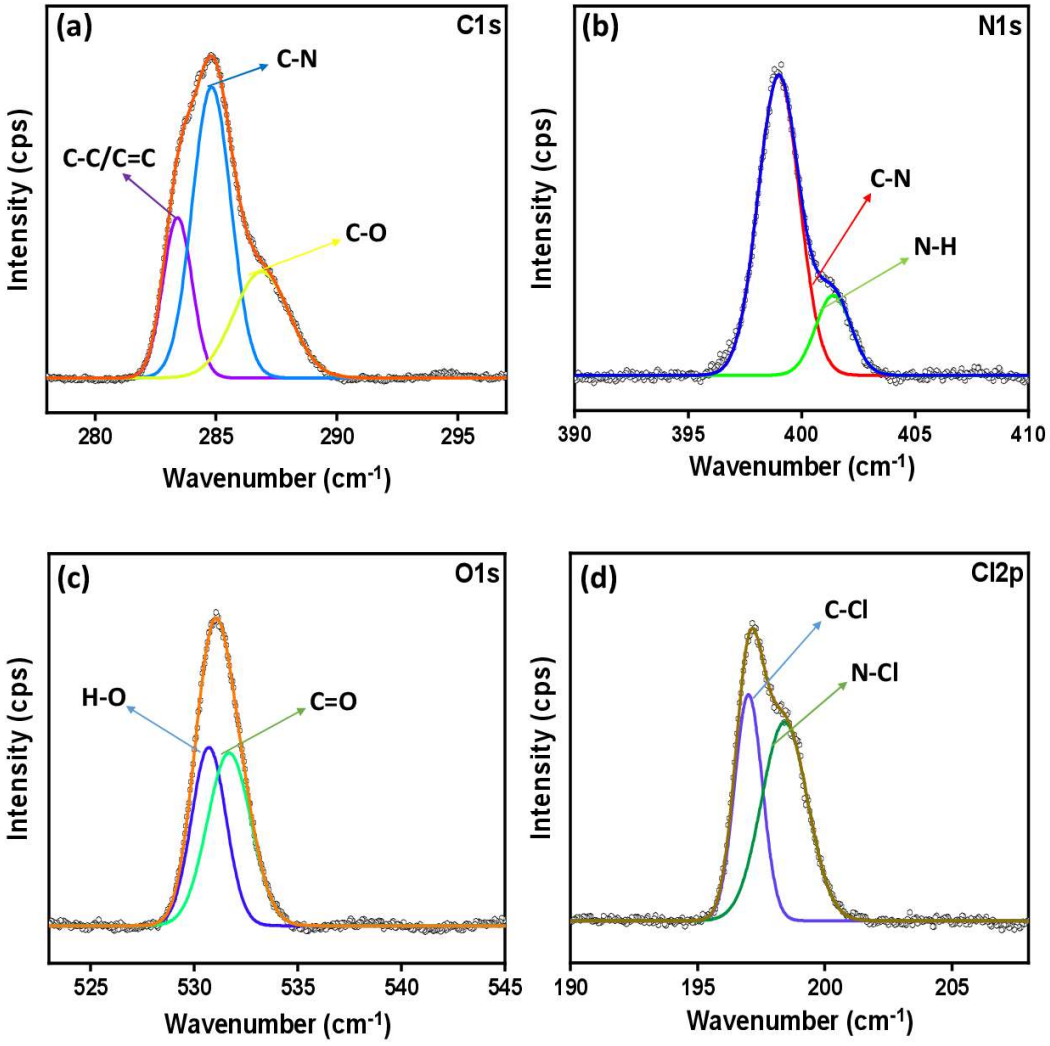

Figure 4.6: (a) XPS graph of C 1s, (b) N 1s, (c) O 1s, (d) Cl 2p of N,Cl-CQDs.

4.3. Optical properties of N,Cl-CQDs

The optical studies of N,Cl-CQDs were done using UV-vis absorption and fluorescence emission spectra at room temperature. The UV-vis spectrum reveals two distinct absorption peaks at 271 and 402 nm (Figure 4.7) that could be ascribed to π-π* transition of C=C bond of the aromatic sp^2 carbon domain[82] and n-π* transition of C=O bond, respectively.[83] Blue colour emission can be seen from the synthesized N,Cl-CQDs when exposed to UV irradiation at 365 nm, as seen in the inset of Figure 4.7, which can also be confirmed by the studies of Commission International de L'Eclairage (CIE). [84] Furthermore, excitation, and emission spectra of N,Cl-CQDs are shown in Figure 4.8a, with peaks near 360 nm and 458 nm, respectively. The PL emission spectra of N,Cl-CQDs under different excitation wavelengths have been shown in Figure 4.8b, which depicts that maximum excitation and emission wavelength were observed at 360 nm and 458 nm, respectively, with a difference of 20 nm. The prepared N,Cl-CQDs display excitation-dependent behaviour in the 300-440 nm range, and a bathochromic shift has been observed between emission wavelengths of 418-500 nm. These findings confirm that N,Cl-CQDs vary in size with diverse organic groups, i.e. NH_2, OH, and COOH, on the surfaces of N,Cl-CQDs, contributing to the emergence of distinct surface emission sites.

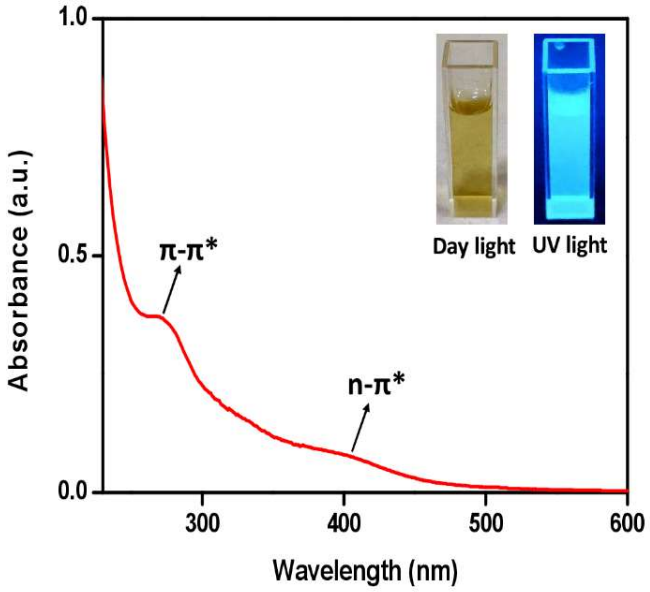

Figure 4.7: UV-vis absorbance spectra of N,Cl-CQDs.

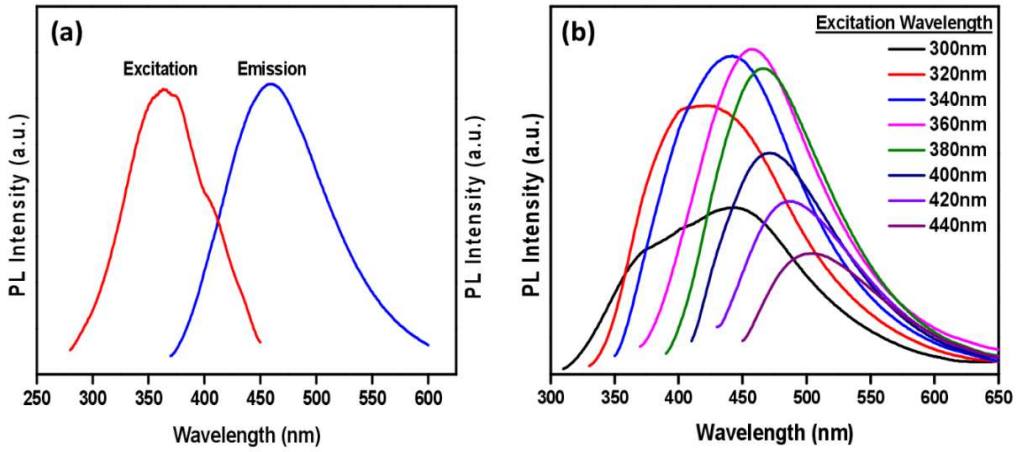

Figure 4.8: (a) PL excitation & emission spectra of N,Cl-CQDs, (b) PL emission spectra of N,Cl-CQDs at different excitation wavelengths ranging from 300-440 nm.

4.4. Optical stability of N,Cl-CQDs

Figure 4.9 illustrates the results of the stability of N,Cl-CQDs under various circumstances, including UV irradiation, storage time, ionic strength and pH. The influence of pH (ranging from pH 3-12) was examined to determine how pH interferes with the PL intensity of N,Cl-CQDs. It has been observed that N,Cl-CQDs exhibited about the same PL intensity at different pH levels (Figure 4.9a), which employs that N,Cl-CQDs can function effectively in both acidic and basic environments. To determine the photostability of the as-prepared N,Cl-CQDs, they were exposed to irradiation under a UV lamp for a duration of 180 minutes (Figure 4.9b). During the course of this exposure period, no substantial change in the fluorescence intensity of N,Cl-CQDs was observed. Additionally, The N,Cl-CQDs were kept in storage for a duration of 40 days, during which PL spectra were regularly measured. The results indicated that there were no observable changes in the PL intensity throughout the entire period (Figure 4.9c). Furthermore, the ionic strength of N,Cl-CQDs were investigated. The varied amounts of NaCl were added to N,Cl-CQDs solution, resulting in a final NaCl concentration of 0–1 M. The results revealed that the PL intensity barely changed as the NaCl concentration changed from 0 to 1 M, and the N,Cl-CQDs were unaffected by a high ion concentration in their surrounding environment (Figure 4.9d). Based on the aforementioned measures, it can be inferred that the N,Cl-CQDs exhibited consistent characteristics and can be utilized to detect Hg^{2+} and GSH.

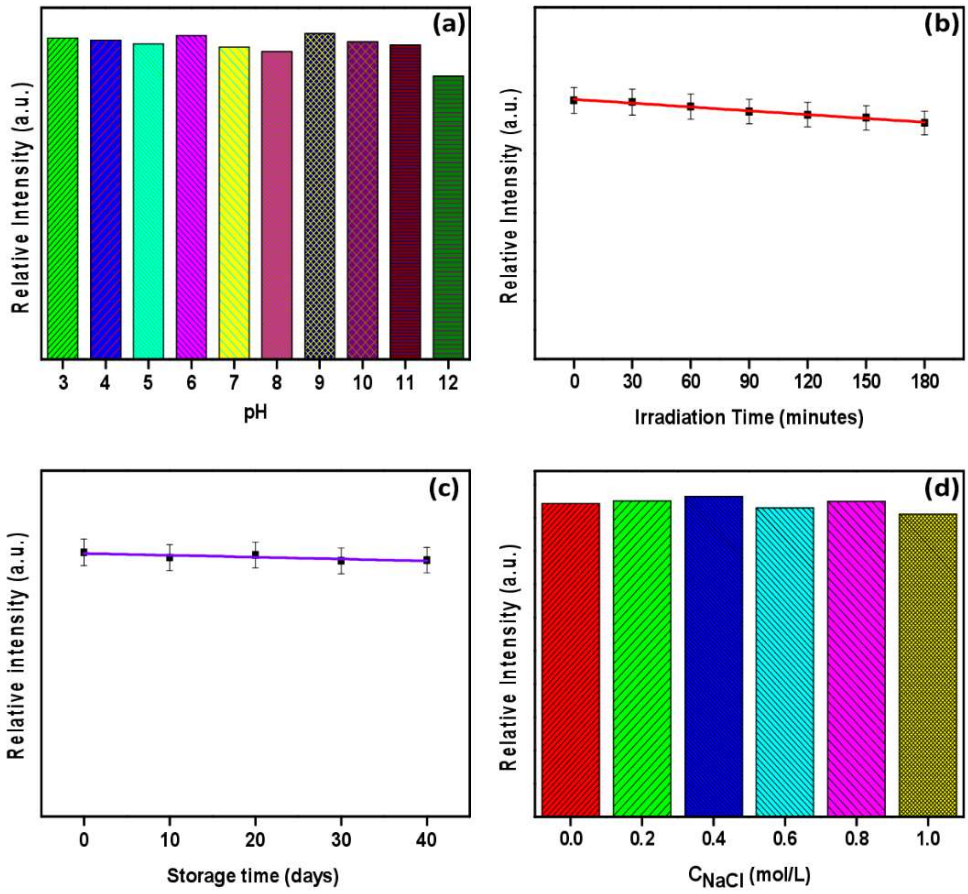

Figure 4.9: Stability of N,Cl-CQDs at different (a) pH values, (b) UV irradiation time (photostability), (c) Storage time and (d) Concentration of NaCl (ionic strength).

4.5. Selectivity towards Hg^{2+}

The assessment of selectivity is a crucial factor in evaluating the efficacy of sensing capabilities of N,Cl-CQDs. To accomplish this, we have analyzed the variation in PL emission intensity caused by the addition of a variety of metal ions that are both ecologically and physiologically significant. These metal ions include Fe^{3+}, K^{+}, Mg^{2+}, Ni^{2+}, Pb^{2+}, Hg^{2+}, Fe^{2+}, Co^{2+}, Cr^{3+}, Ba^{2+}, Cu^{2+}, Mn^{2+} and NH_4^+ ions of the same concentration. The PL emission spectra of the N,Cl-CQDs with different metal ions solutions are subsequently measured and observed. Based on the data presented in Figure 4.10a, it is evident that most ions have a minimal impact on emission, except for Hg^{2+}. Furthermore, the interference studies of the prepared system were also carried out for greater selectivity by combining Hg^{2+} ions with other metal ions in a ratio of 1:3, and it was discovered that other metal ions did not significantly interfere with Hg^{2+} ions (Figure 4.10b).

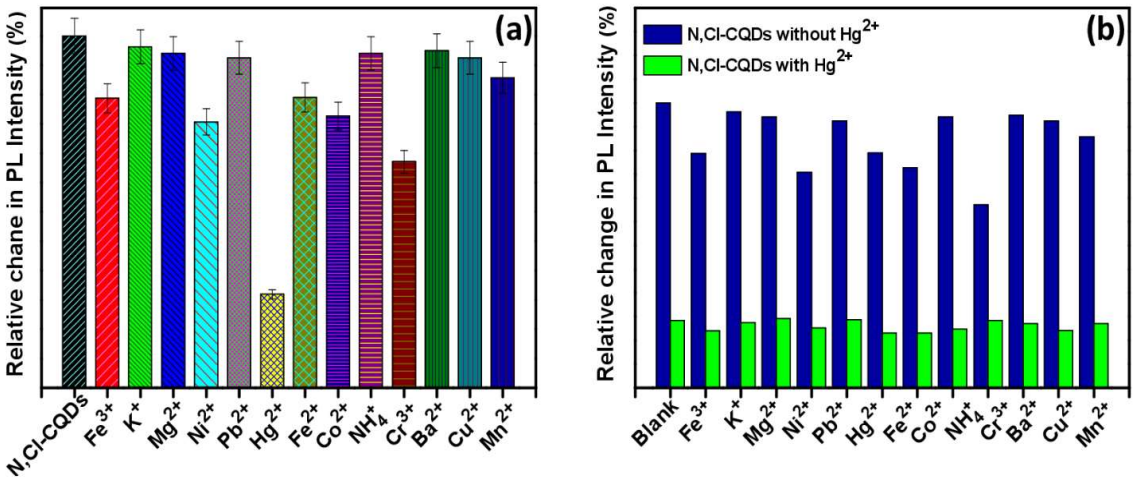

Figure 4.10: (a) Selectivity studies of N,Cl-CQDs with different metal ions, (b) Interference study of N,Cl-CQDs for Hg^{2+} in the presence of different metal ions.

4.6. Detection of Hg^{2+}

To illustrate the sensitivity of prepared N,Cl-CQDs for Hg^{2+} ions, the variable concentrations of Hg^{2+} ions (ranging from 0 µM to 0.85 µM) were added to the fluorescent probe, and it has been found that the PL intensity steadily reduced (turn-off) as the concentration of Hg^{2+} increased (Figure 4.11a). To analyze and understand the PL quenching response of the developed fluorescence sensing probe (N,Cl-CQDs) with the addition of Hg^{2+} ions as a quencher, the Stern-Volmer graph was plotted using the equation (2):

$$\frac{F_0}{F} = 1 + K_{sv}\,[Q] \qquad (2)$$

Where "F_0" and "F" represent PL intensity of N,Cl-CQDs without quencher and with quencher (Hg^{2+}), respectively, and K_{sv} denotes the Stern-Volmer quenching constant, which was determined to be 4.1×10^6 M^{-1} with an R^2 value of 0.985 (Figure 4.11b). Furthermore, it was found that the value of $F_0 - F/F_0$ exhibited a strong linear correlation with the concentration of Hg^{2+} within the range of 0 to 0.85 µM with the R^2 value of 0.976 (Figure 4.12). The inset figure in Figure 4.9c indicates a linear correlation ($F_0 - F/F_0 = 1.32876[Hg^{2+}] + 0.02947$) between the values of $F_0 - F/F_0$ and concentrations of Hg^{2+} ions (0 to 0.35 µM) with an R^2 value of 0.995; using this plot, the calculation of the limit of detection (LOD) for Hg^{2+} was done using 3σ/k rule, where "σ" indicates the standard deviation of intercept and "k" indicates slope of linear equation, the calculated value of LOD for Hg^{2+} found to be 39 nM. In comparison to the fluorescent probes for Hg^{2+} discussed in the literature (refer to Table 4.1),

The N,Cl-CQDs synthesized in our study offer a highly efficient platform with enhanced sensitivity and a broad detection range for Hg^{2+} detection.

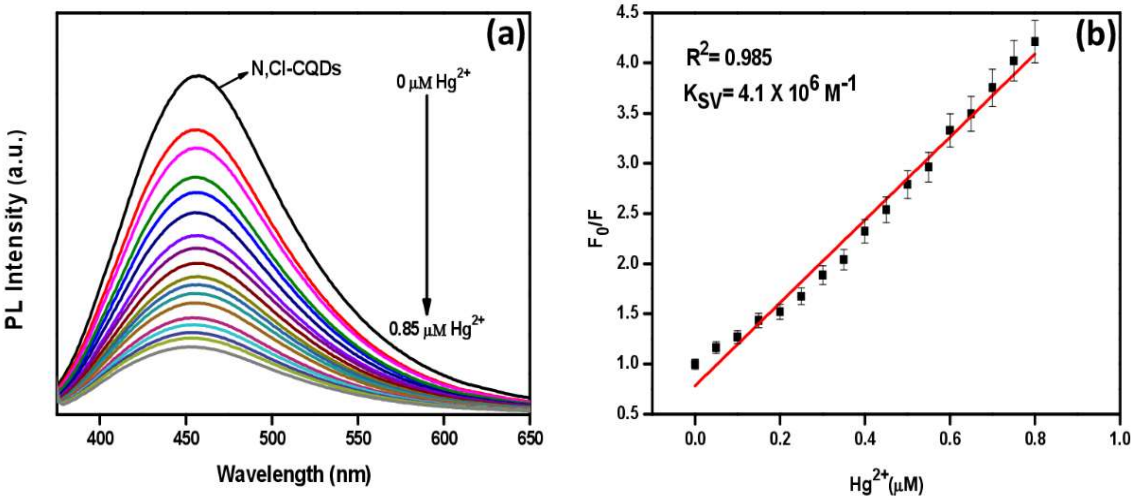

Figure 4.11: (a) Effect of different concentrations of Hg^{2+} on the PL intensity of N,Cl-CQDs, (b) The Stern-Volmer plot between F_0/F & different concentrations of Hg^{2+} ions.

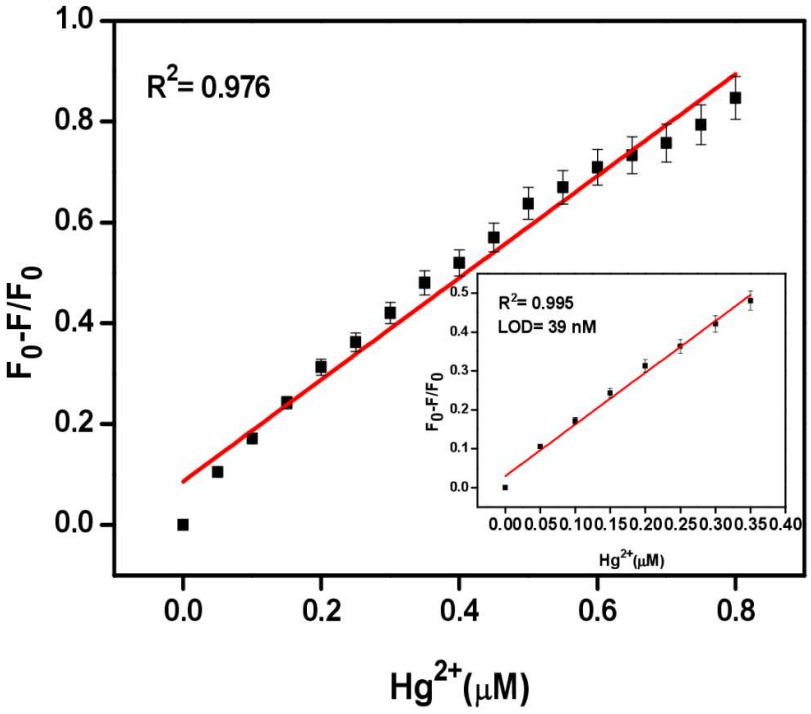

Figure 4.12: Linear correlation between F_0-F/F_0 & different concentrations of Hg^{2+} (0 to 0.85 μM) with inset image of concentrations of Hg^{2+} (0 to 0.35).

Table 4.1: Comparative study of different sensing systems for detecting Hg^{2+} ions.

Sensing Systems	Detection Range	LOD	Reference
CD-1 and CD-2	1-12 µM and 1-15 µM	226 nM and 845 nM	[85]
CDs	2 to 14 µM	0.44 µM	[86]
NCDs	0.001 to 5 µM	0.65 µM	[87]
N-S-C-dots	0 to 40 µM	2 µM	[88]
N-CQDs	0 to 25 µM	0.23 µM	[89]
N-CDs	10 to 160 µM	0.48 µM	[90]
PNBS-CQDs	25 to 1500 µM	5.0 µM	[91]
N-CQDs	0.2 to 1.2 µM	0.085 µM	[92]
La-CQDs	0.5 to 40 µM	0.1 µM	[93]
Dual-CD	0 to 60 µM	477 nM	[94]
N,Cl-CQDs	0 to 0.35 µM	39 nM	Present work

4.7. Recovery of N,Cl-CQDs by GSH

4.7.1. Selectivity towards GSH

The fluorescence of N,Cl-CQDs has been discovered to undergo quenching in the presence of Hg^{2+} ions. However, it remains to be determined whether the PL intensity of N,Cl-CQDs + Hg^{2+} can be restored or not. Therefore, in this study, a range of small biomolecules, i.e. arginine (Arg), methionine (Met), leucine (Leu), histidine (His), dopamine (DA), asparagine (Asn), glutathione (GSH), valine (Val), glutamic acid (Glu), glutamine (Gln), lysine (Lys), alanine (Ala), glucose (Glc), cysteine (Cys), aspartic acid (Asp), isoleucine (Ile), threonine (Thr) of same concentration was added to the N,Cl-CQDs + Hg^{2+} system to explore fluorescence recovery. The results revealed that only GSH could regain the fluorescence; other compounds could not (Figure 4.13a). The fluorescence recovery exhibited greater prominence following the introduction of GSH. Furthermore, the interference studies of N,Cl-CQDs + Hg^{2+} sensing system for GSH were also carried out by adding GSH and other biomolecules in a ratio of 1:3, as shown in Figure 4.13b. The results reveal that the system under investigation exhibits a significant degree of selectivity towards GSH compared to the other biomolecules.

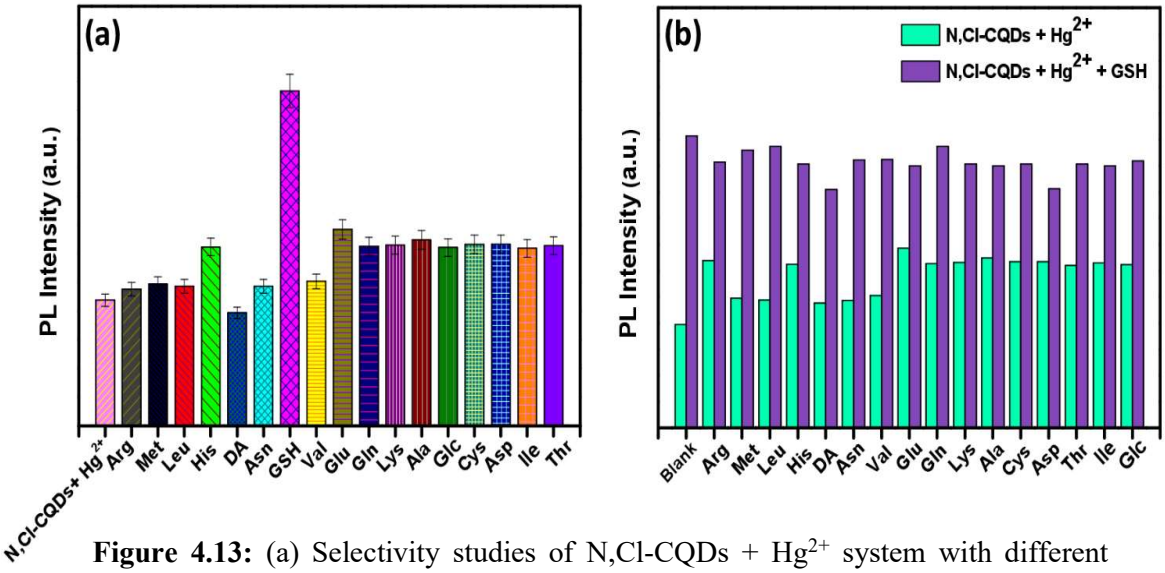

Figure 4.13: (a) Selectivity studies of N,Cl-CQDs + Hg^{2+} system with different biomolecules, (b) Interference study of N,Cl-CQDs + Hg^{2+} system for GSH in the presence of different biomolecules.

4.7.2. Detection of GSH

Selectivity studies showed that N,Cl-CQDs + Hg^{2+} system has the potential to function as a highly effective sensing system for the detection of GSH by using the turn "off-on" mechanism. The fluorescence recovery of N,Cl-CQDs + Hg^{2+} was achieved by adding varying concentrations of GSH (ranging from 0 to 5.5 µM) into the N,Cl-CQDs + Hg^{2+} sensing system; the results revealed that fluorescence intensity gradually enhanced (turn-on) as the concentration of GSH increased (Figure 4.14a). The PL intensity exhibited a recovery of 86% upon adding 5.5 µM of GSH. Furthermore, no apparent change in the PL intensity of N,Cl-CQDs was noticed with increasing amounts of GSH beyond 5.5 µM. The correlation between the value of $F - F_0/F_0$ and the GSH concentration ranging from 0 to 0.60 µM exhibited a high degree of linearity ($F_0 - F/F_o = 0.9126[GSH] + 0.00347$) with an R^2 value of 0.998 (Figure 4.14b). The LOD of GSH was calculated to be 43 nM (using the 3σ/k method), proving that the prepared sensing system had a lower detection limit than other glutathione (GSH) probes, as shown in Table 4.2

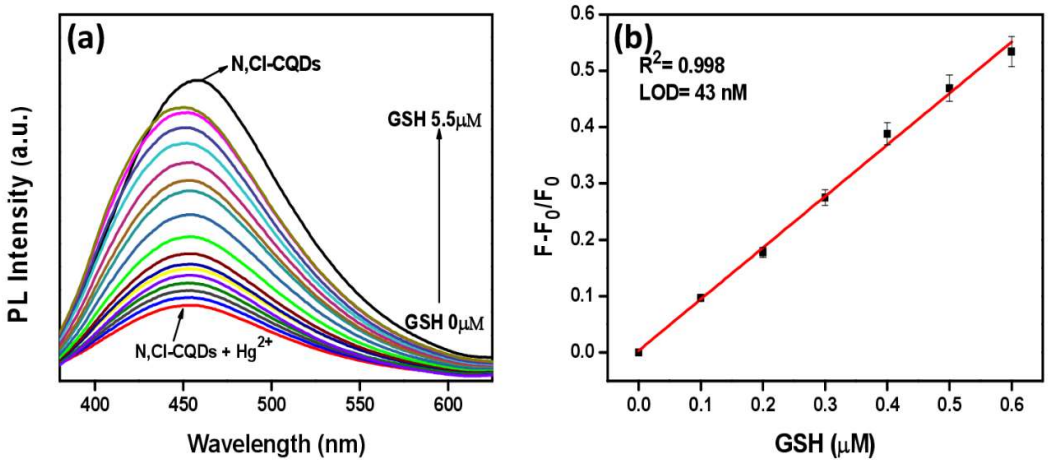

Figure 4.14: (a) Effect of different concentrations of GSH on the PL intensity of N,Cl-CQDs + Hg^{2+} sensing system, (b) Linear correlation between F_0-F/F_0 & different concentrations of GSH (0 to 0.60 μM).

Table 4.2: Comparative study of different sensing systems for the detection of GSH.

Sensing Systems	**Detection Range**	**LOD**	**Reference**
BN-CDs/Hg^{2+}	5 to 200 μM	1.7 μM	[95]
CDs-Hg^{2+}	0 to 60 μM	0.3 μM	[96]
CDs-Cu^{2+}	20 to 400 μM	5.98 μM	[97]
C-dots-MnO_2	1 to 10 μM	300 nM	[98]
Au(III)/CDC	0 to 150 μM	2.02 μM	[99]
N-CDs/Fe^{3+}	0 to 67 μM	0.226 μM	[100]
N-CQDs + Hg^{2+}	5 to 30 μM	2 μM	[101]
SNCDs	10 to 460 μM	0.25 μM	[102]
EDC/CQDs	1.0 to 50 μM	0.943 μM	[103]
wCDs	0 to 3.0 mM	35 μM	[104]
N,Cl-CQDs + Hg^{2+}	0 to 0.60 μM	43 nM	Present work

4.8. Plausible Sensing Mechanism

The predominant fluorescence quenching mechanisms consist of static quenching, dynamic quenching, photoinduced electron transfer (PET), inner filter effect (IFE) and as well as fluorescence resonance energy transfer (FRET).[105,106] When a fluorescent molecule interacts with a quencher, the development of a ground-state non-fluorescent complex causes static quenching. On the other hand, dynamic quenching takes place as a result of the collision between a fluorescent molecule and a quencher while in the excited state, and the complex formed subsequently returns to the ground state through charge transfer.[107108] In fluorescence lifetime measurements, the ratio between the lifetime of the excited state complex and the ground state complex is equivalent to one ($\tau_0/\tau = 1$), which suggests the static quenching mechanism. In Contrast, in the dynamic quenching mechanism, the fluorescence lifetime varies depending on whether a quencher is present or not. In this study, The UV–vis peak of absorption showed very little difference due to the presence of Hg^{2+} (Figure 4.15a). Alongside the fact that the fluorescent emission and excitation wavelengths remained unaffected by the presence of Hg^{2+} (as depicted in Figure 4.11a), these results indicate the absence of both fluorescence resonance energy transfer (FRET) and inner filter effect (IFE). The fluorescence lifetime decay (tri-exponential fit) of N,Cl-CQDs in the absence and presence of Hg^{2+} was determined to be 1.69 and 0.97 ns, respectively. After GSH was added in the N,Cl-CQDs + Hg^{2+} system, the obtained fluorescence lifetime was 1.23 ns (Figure 4.15b). The findings of this study indicate that the fluorescence quenching of N,Cl-CQDs occurred via a dynamic quenching mechanism.[109–111] Furthermore, the zeta potential measurements were also used to investigate the quenching mechanism. The zeta potential values (Figure 4.16) for the N,Cl-CQDs were determined to be -14.03 mV. The observed negative potential of N,Cl-CQDs may be attributed to numerous hydroxyl (-OH), amino ($-NH_2$) and carboxyl (-COOH) functional groups exposed on the surface of the N,Cl-CQDs. After the addition of Hg^{2+}, the value of zeta potential increased to +8.48 mV, and the positive zeta potential of N,Cl-CQDs + Hg^{2+} suggests that -OH groups bind to Hg^{2+} to form a non-fluorescent complex.[112] Further, after GSH was added in N,Cl-CQDs + Hg^{2+} system, the zeta potential decreased to -5.09 mV. This could be due to significant interaction between Hg^{2+} and sulfhydryl groups which leads to the elimination of Hg^{2+} from the surfaces of N,Cl-CQDs. Furthermore, the mechanism behind fluorescence recovery can be elucidated in the following manner, which was also validated by lifetime data, the ability of Hg^{2+} to form complexes with GSH exhibited higher resilience compared to its ability to form complexes with N,Cl-CQDs. Based on the HSAB principle, it

can be implied that Hg^{2+} shows a higher tendency to form bonds with sulfhydryl groups attached to GSH.[113] As a result, the N,Cl-CQDs and Hg^{2+} ions were effectively separated and ofregained from the N,Cl-CQDs + Hg^{2+} complex upon the addition of GSH, which leads to the fluorescence recovery (Figure 4.17).

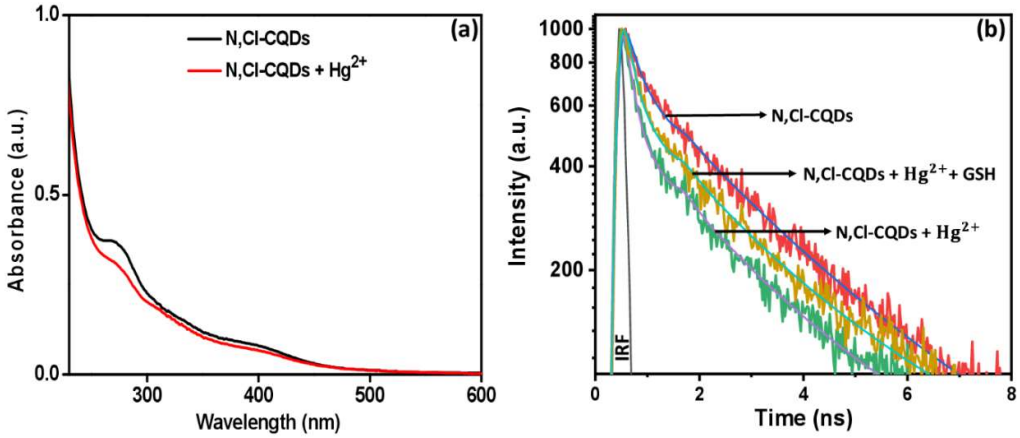

Figure 4.15: (a) UV-vis absorbance spectra of N,Cl-CQDs without Hg^{2+} and with Hg^{2+}, (b) Fluorescence lifetime studies of N,Cl-CQDs in the presence of Hg^{2+} and GSH.

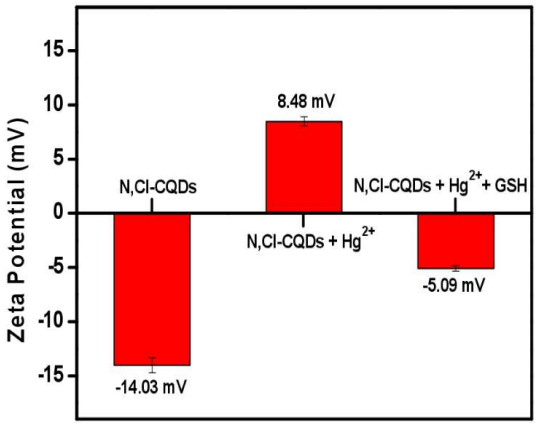

Figure 4.16: Zeta potential values of N,Cl-CQDs in the presence of Hg^{2+} and GSH.

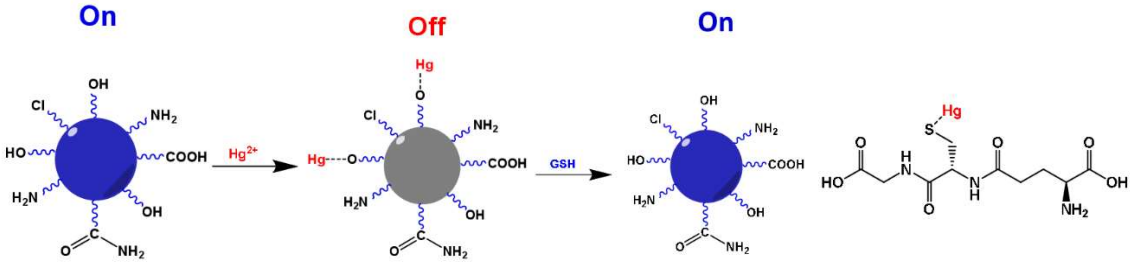

Figure 4.17: Plausible turn "On-Off-On" mechanism of N,Cl-CQDs.

Furthermore, the quantum yield of N,Cl-CQDs with Hg^{2+} and GSH has been calculated using equation (1) and represented in Table 4.3. The addition of Hg^{2+} ions decreased the QY of N,Cl-CQDs from 36% to 12%, while the addition of GSH resulted in the restoration of the QY of N,Cl-CQDs from 12% to 31%. Further, By using data of quantum yield and fluorescence lifetime decays, the photophysical parameters of N,Cl-CQDs have been calculated and represented in Table 4.3. Additionally, to illustrate the mechanism of fluorescence quenching, we have computed the value of the radiative rate constant (k_r) and non-radiative rate constant (k_{nr})[114] using the following equation:

$$k_r = \frac{\phi_f}{\tau_f} \quad (3)$$

$$\frac{1}{\tau_f} = k_r + k_{nr} \quad (4)$$

Where "τ_f" represents the average lifetime value, and "ϕ_f" depicts fluorescence quantum yield. From Table 4.3, it has been noticed that with the addition of Hg^{2+}, the value of k_r is decreasing, and the value of knr is increasing, which implies that the PL quenching mechanism also involves excited-state electron transfer.[115]

Table 4.3: Photophysical parameters of N,Cl-CQDs with of Hg^{2+} ions and GSH.

System	**Φ**	**#<τ_{avg}> (ns)**	**k_r (10^9 s^{-1})**	**k_{nr} (10^9 s^{-1})**
un-doped CQDs	0.15	-	-	-
N,Cl-CQDs	0.36	1.69	0.21	0.38
N,Cl-CQDs + Hg^{2+}	0.12	0.97	0.12	0.91
N,Cl-CQDs + Hg^{2+} + GSH	0.31	1.23	0.25	0.56

#<τ_{avg}> = $a_1\tau_1 + a_2\tau_2 + a_3\tau_3$

CONCLUSION

In conclusion, the nitrogen & chloride co-doped carbon quantum dots (N,Cl-CQDs) were prepared using choline chloride-urea based green solvent and wheatgrass as a precursor via a facile, green, faster and more cost-effective microwave synthesis approach. The N,Cl-CQDs exhibited a high quantum yield of 36%. The structural morphology and size of the N,Cl-CQDs were determined using TEM images, and their elemental compositions were confirmed by XPS analysis. The prepared N,Cl-CQDs shows high fluorescence intensity with good water solubility, pH stability, and high photostability. The fluorescence intensity of N,Cl-CQDs was quenched by Hg^{2+} (turn-off) and then restored after the addition of GSH (turn-on). The limit of detection for Hg^{2+} and GSH were found to be 39 nM and 43 nM, respectively. Further, Hg^{2+} decreases the quantum yield and average lifetime of N,Cl-CQDs which suggests dynamic quenching mechanism between the N,Cl-CQDs and Hg^{2+} ions. The increased zeta potential values of N,Cl-QDs + Hg^{2+} system revealed the strong affinity between Hg^{2+} and sulfhydryl group of GSH which may leads to fluorescence recovery of N,Cl-CQDs. Among the wide range of sensing probes available, the suggested sensing system exhibits rapid response, cost-effectiveness, environmental compatibility, and a remarkable detection limit for Hg^{2+} ions and GSH via an “On-Off-On” mechanism.

REFERENCES

(1) Xu, X.; Ray, R.; Gu, Y.; Ploehn, H. J.; Gearheart, L.; Raker, K.; Scrivens, W. A. Electrophoretic Analysis and Purification of Fluorescent Single-Walled Carbon Nanotube Fragments. *J Am Chem Soc* **2004**, *126* (40), 12736–12737. https://doi.org/10.1021/ja040082h.

(2) Das, T.; Saikia, B. K.; Dekaboruah, H. P.; Bordoloi, M.; Neog, D.; Bora, J. J.; Lahkar, J.; Narzary, B.; Roy, S.; Ramaiah, D. Blue-Fluorescent and Biocompatible Carbon Dots Derived from Abundant Low-Quality Coals. *J Photochem Photobiol B* **2019**, *195*, 1–11. https://doi.org/10.1016/j.jphotobiol.2019.04.004.

(3) Vibhute, A.; Patil, T.; Gambhir, R.; Tiwari, A. P. Fluorescent Carbon Quantum Dots: Synthesis Methods, Functionalization and Biomedical Applications. *Applied Surface Science Advances* **2022**, *11*, 100311. https://doi.org/10.1016/j.apsadv.2022.100311.

(4) Gan, Z.; Xu, H.; Hao, Y. Mechanism for Excitation-Dependent Photoluminescence from Graphene Quantum Dots and Other Graphene Oxide Derivates: Consensus, Debates and Challenges. *Nanoscale* **2016**, *8* (15), 7794–7807. https://doi.org/10.1039/C6NR00605A.

(5) Majood, M.; Garg, P.; Chaurasia, R.; Agarwal, A.; Mohanty, S.; Mukherjee, M. Carbon Quantum Dots for Stem Cell Imaging and Deciding the Fate of Stem Cell Differentiation. *ACS Omega* **2022**, *7* (33), 28685–28693. https://doi.org/10.1021/acsomega.2c03285.

(6) Soumya, K.; More, N.; Choppadandi, M.; Aishwarya, D. A.; Singh, G.; Kapusetti, G. A Comprehensive Review on Carbon Quantum Dots as an Effective Photosensitizer and Drug Delivery System for Cancer Treatment. *Biomedical Technology* **2023**, *4*, 11–20. https://doi.org/10.1016/j.bmt.2023.01.005.

(7) Carneiro, S. V.; de Queiroz, V. H. R.; Cruz, A. A. C.; Fechine, L. M. U. D.; Denardin, J. C.; Freire, R. M.; do Nascimento, R. F.; Fechine, P. B. A. Sensing Strategy Based on Carbon Quantum Dots Obtained from Riboflavin for the Identification of Pesticides. *Sens Actuators B Chem* **2019**, *301*, 127149. https://doi.org/10.1016/j.snb.2019.127149.

(8) Liu, M.; Xu, Y.; Niu, F.; Gooding, J. J.; Liu, J. Carbon Quantum Dots Directly Generated from Electrochemical Oxidation of Graphite Electrodes in Alkaline Alcohols and the Applications for Specific Ferric Ion Detection and Cell Imaging. *Analyst* **2016**, *141* (9), 2657–2664. https://doi.org/10.1039/C5AN02231B.

(9) Shafique, M.; Mahr, M. S.; Yaseen, M.; Bhatti, H. N. CQD/TiO2 Nanocomposite Photocatalyst for Efficient Visible Light-Driven Purification of Wastewater Containing Methyl Orange Dye. *Mater Chem Phys* **2022**, *278*, 125583. https://doi.org/10.1016/j.matchemphys.2021.125583.

(10) Sikiru, S.; Oladosu, T. L.; Kolawole, S. Y.; Mubarak, L. A.; Soleimani, H.; Afolabi, L. O.; Oluwafunke Toyin, A.-O. Advance and Prospect of Carbon Quantum Dots Synthesis for Energy Conversion and Storage Application: A Comprehensive Review. *J Energy Storage* **2023**, *60*, 106556. https://doi.org/10.1016/j.est.2022.106556.

(11) Chahal, S.; Yousefi, N.; Tufenkji, N. Green Synthesis of High Quantum Yield Carbon Dots from Phenylalanine and Citric Acid: Role of Stoichiometry and Nitrogen Doping. *ACS Sustain Chem Eng* **2020**, *8* (14), 5566–5575. https://doi.org/10.1021/acssuschemeng.9b07463.

(12) Uriarte, D.; Domini, C.; Garrido, M. New Carbon Dots Based on Glycerol and Urea and Its Application in the Determination of Tetracycline in Urine Samples. *Talanta* **2019**, *201*, 143–148. https://doi.org/10.1016/j.talanta.2019.04.001.

(13) Roy, P.; Periasamy, A. P.; Chuang, C.; Liou, Y. R.; Chen, Y. F.; Joly, J.; Liang, C. Te; Chang, H. T. Plant Leaf-Derived Graphene Quantum Dots and Applications for White LEDs. *New Journal of Chemistry* **2014**, *38* (10), 4946–4951. https://doi.org/10.1039/c4nj01185f.

(14) Mathew, S. A.; Praveena, P.; Dhanavel, S.; Manikandan, R.; Senthilkumar, S.; Stephen, A. Luminescent Chitosan/Carbon Dots as an Effective Nano-Drug Carrier for Neurodegenerative Diseases. *RSC Adv* **2020**, *10* (41), 24386–24396. https://doi.org/10.1039/D0RA04599C.

(15) Guan, X.; Li, Z.; Geng, X.; Lei, Z.; Karakoti, A.; Wu, T.; Kumar, P.; Yi, J.; Vinu, A. Emerging Trends of Carbon-Based Quantum Dots: Nanoarchitectonics and Applications. *Small* **2023**, *19* (17). https://doi.org/10.1002/smll.202207181.

(16) Liu, J.; Li, R.; Yang, B. Carbon Dots: A New Type of Carbon-Based Nanomaterial with Wide Applications. *ACS Cent Sci* **2020**, *6* (12), 2179–2195. https://doi.org/10.1021/acscentsci.0c01306.

(17) Zulfajri, M.; Abdelhamid, H. N.; Sudewi, S.; Dayalan, S.; Rasool, A.; Habib, A.; Huang, G. G. Plant Part-Derived Carbon Dots for Biosensing. *Biosensors (Basel)* **2020**, *10* (6), 68. https://doi.org/10.3390/bios10060068.

(18) Ma, X.; Dong, Y.; Sun, H.; Chen, N. Highly Fluorescent Carbon Dots from Peanut Shells as Potential Probes for Copper Ion: The Optimization and Analysis of the Synthetic Process. *Mater Today Chem* **2017**, *5*, 1–10. https://doi.org/10.1016/j.mtchem.2017.04.004.

(19) Kundu, A.; Maity, B.; Basu, S. Rice Husk-Derived Carbon Quantum Dots-Based Dual-Mode Nanoprobe for Selective and Sensitive Detection of Fe^{3+} and Fluoroquinolones. *ACS Biomater Sci Eng* **2022**, *8* (11), 4764–4776. https://doi.org/10.1021/acsbiomaterials.2c00798.

(20) Kundu, A.; Maity, B.; Basu, S. Orange Pomace-Derived Fluorescent Carbon Quantum Dots: Detection of Dual Analytes in the Nanomolar Range. *ACS Omega* **2023**, *8* (24), 22178–22189. https://doi.org/10.1021/acsomega.3c02474.

(21) Singh, J.; Kaur, S.; Lee, J.; Mehta, A.; Kumar, S.; Kim, K.-H.; Basu, S.; Rawat, M. Highly Fluorescent Carbon Dots Derived from Mangifera Indica Leaves for Selective Detection of Metal Ions. *Science of The Total Environment* **2020**, *720*, 137604. https://doi.org/10.1016/j.scitotenv.2020.137604.

(22) Huang, Z.-Y.; Wu, W.-Z.; Li, Z.-X.; Wu, Y.; Wu, C.-B.; Gao, J.; Guo, J.; Chen, Y.; Hu, Y.; Huang, C. Solvothermal Production of Tea Residue Derived Carbon Dots by the Pretreatment of Choline Chloride/Urea and Its Application for Cadmium Detection. *Ind Crops Prod* **2022**, *184*, 115085. https://doi.org/10.1016/j.indcrop.2022.115085.

(23) Atchudan, R.; Jebakumar Immanuel Edison, T. N.; Shanmugam, M.; Perumal, S.; Somanathan, T.; Lee, Y. R. Sustainable Synthesis of Carbon Quantum Dots from Banana Peel Waste Using Hydrothermal Process for in Vivo Bioimaging. *Physica E Low Dimens Syst Nanostruct* **2021**, *126*, 114417. https://doi.org/10.1016/j.physe.2020.114417.

(24) Gedda, G.; Sankaranarayanan, S. A.; Putta, C. L.; Gudimella, K. K.; Rengan, A. K.; Girma, W. M. Green Synthesis of Multi-Functional Carbon Dots from Medicinal Plant Leaves for

Antimicrobial, Antioxidant, and Bioimaging Applications. *Sci Rep* **2023**, *13* (1), 6371. https://doi.org/10.1038/s41598-023-33652-8.

(25) Manzoor, S.; Dar, A. H.; Dash, K. K.; Pandey, V. K.; Srivastava, S.; Bashir, I.; Khan, S. A. Carbon Dots Applications for Development of Sustainable Technologies for Food Safety: A Comprehensive Review. *Applied Food Research* **2023**, *3* (1), 100263. https://doi.org/10.1016/j.afres.2023.100263.

(26) Chao-Mujica, F. J.; Garcia-Hernández, L.; Camacho-López, S.; Camacho-López, M.; Camacho-López, M. A.; Reyes Contreras, D.; Pérez-Rodríguez, A.; Peña-Caravaca, J. P.; Páez-Rodríguez, A.; Darias-Gonzalez, J. G.; Hernandez-Tabares, L.; Arias de Fuentes, O.; Prokhorov, E.; Torres-Figueredo, N.; Reguera, E.; Desdin-García, L. F. Carbon Quantum Dots by Submerged Arc Discharge in Water: Synthesis, Characterization, and Mechanism of Formation. *J Appl Phys* **2021**, *129* (16), 163301. https://doi.org/10.1063/5.0040322.

(27) Kaczmarek, A.; Hoffman, J.; Morgiel, J.; Mościcki, T.; Stobiński, L.; Szymański, Z.; Małolepszy, A. Luminescent Carbon Dots Synthesized by the Laser Ablation of Graphite in Polyethylenimine and Ethylenediamine. *Materials* **2021**, *14* (4), 729. https://doi.org/10.3390/ma14040729.

(28) Sharma, A.; Das, J. Small Molecules Derived Carbon Dots: Synthesis and Applications in Sensing, Catalysis, Imaging, and Biomedicine. *J Nanobiotechnology* **2019**, *17* (1), 92. https://doi.org/10.1186/s12951-019-0525-8.

(29) Modi, P. D.; Mehta, V. N.; Prajapati, V. S.; Patel, S.; Rohit, J. V. Bottom-up Approaches for the Preparation of Carbon Dots. In *Carbon Dots in Analytical Chemistry*; Elsevier, 2023; pp 15–29. https://doi.org/10.1016/B978-0-323-98350-1.00022-0.

(30) Yang, H.-L.; Bai, L.-F.; Geng, Z.-R.; Chen, H.; Xu, L.-T.; Xie, Y.-C.; Wang, D.-J.; Gu, H.-W.; Wang, X.-M. Carbon Quantum Dots: Preparation, Optical Properties, and Biomedical Applications. *Mater Today Adv* **2023**, *18*, 100376. https://doi.org/10.1016/j.mtadv.2023.100376.

(31) Ng, H. K. M.; Lim, G. K.; Leo, C. P. Comparison between Hydrothermal and Microwave-Assisted Synthesis of Carbon Dots from Biowaste and Chemical for Heavy Metal Detection: A Review. *Microchemical Journal* **2021**, *165*, 106116. https://doi.org/10.1016/j.microc.2021.106116.

(32) de Medeiros, T. V.; Manioudakis, J.; Noun, F.; Macairan, J.-R.; Victoria, F.; Naccache, R. Microwave-Assisted Synthesis of Carbon Dots and Their Applications. *J Mater Chem C Mater* **2019**, *7* (24), 7175–7195. https://doi.org/10.1039/C9TC01640F.

(33) Kumar, P.; Dua, S.; Kaur, R.; Kumar, M.; Bhatt, G. A Review on Advancements in Carbon Quantum Dots and Their Application in Photovoltaics. *RSC Adv* **2022**, *12* (8), 4714–4759. https://doi.org/10.1039/D1RA08452F.

(34) Sun, Y.-P.; Zhou, B.; Lin, Y.; Wang, W.; Fernando, K. A. S.; Pathak, P.; Meziani, M. J.; Harruff, B. A.; Wang, X.; Wang, H.; Luo, P. G.; Yang, H.; Kose, M. E.; Chen, B.; Veca, L. M.; Xie, S.-Y. Quantum-Sized Carbon Dots for Bright and Colorful Photoluminescence. *J Am Chem Soc* **2006**, *128* (24), 7756–7757. https://doi.org/10.1021/ja062677d.

(35) John, V. L.; Nair, Y.; Vinod, T. P. Doping and Surface Modification of Carbon Quantum Dots for Enhanced Functionalities and Related Applications. *Particle & Particle Systems Characterization* **2021**, *38* (11), 2100170. https://doi.org/10.1002/ppsc.202100170.

(36) Lin, L.; Luo, Y.; Tsai, P.; Wang, J.; Chen, X. Metal Ions Doped Carbon Quantum Dots: Synthesis, Physicochemical Properties, and Their Applications. *TrAC Trends in Analytical Chemistry* **2018**, *103*, 87–101. https://doi.org/10.1016/j.trac.2018.03.015.

(37) Zheng, J.; Xie, Y.; Wei, Y.; Yang, Y.; Liu, X.; Chen, Y.; Xu, B. An Efficient Synthesis and Photoelectric Properties of Green Carbon Quantum Dots with High Fluorescent Quantum Yield. *Nanomaterials* **2020**, *10* (1), 82. https://doi.org/10.3390/nano10010082.

(38) Abbott, A. P.; Capper, G.; Davies, D. L.; Rasheed, R. K.; Tambyrajah, V. Novel Solvent Properties of Choline Chloride/Urea MixturesElectronic Supplementary Information (ESI) Available: Spectroscopic Data. See Http://Www.Rsc.Org/Suppdata/Cc/B2/B210714g/. *Chemical Communications* **2003**, No. 1, 70–71. https://doi.org/10.1039/b210714g.

(39) Santana-Mayor, Á.; Rodríguez-Ramos, R.; Herrera-Herrera, A. V.; Socas-Rodríguez, B.; Rodríguez-Delgado, M. Á. Deep Eutectic Solvents. The New Generation of Green Solvents in Analytical Chemistry. *TrAC Trends in Analytical Chemistry* **2021**, *134*, 116108. https://doi.org/10.1016/j.trac.2020.116108.

(40) Lei, Z.; Chen, B.; Koo, Y.-M.; MacFarlane, D. R. Introduction: Ionic Liquids. *Chem Rev* **2017**, *117* (10), 6633–6635. https://doi.org/10.1021/acs.chemrev.7b00246.

(41) Płotka-Wasylka, J.; de la Guardia, M.; Andruch, V.; Vilková, M. Deep Eutectic Solvents vs Ionic Liquids: Similarities and Differences. *Microchemical Journal* **2020**, *159*, 105539. https://doi.org/10.1016/j.microc.2020.105539.

(42) Smith, E. L.; Abbott, A. P.; Ryder, K. S. Deep Eutectic Solvents (DESs) and Their Applications. *Chem Rev* **2014**, *114* (21), 11060–11082. https://doi.org/10.1021/cr300162p.

(43) Wang, M.; Kang, X.; Deng, L.; Wang, M.; Xia, Z.; Gao, D. Deep Eutectic Solvent Assisted Synthesis of Carbon Dots Using Sophora Flavescens Aiton Modified with Polyethyleneimine: Application in Myricetin Sensing and Cell Imaging. *Food Chem* **2021**, *345*, 128817. https://doi.org/10.1016/j.foodchem.2020.128817.

(44) Hansen, B. B.; Spittle, S.; Chen, B.; Poe, D.; Zhang, Y.; Klein, J. M.; Horton, A.; Adhikari, L.; Zelovich, T.; Doherty, B. W.; Gurkan, B.; Maginn, E. J.; Ragauskas, A.; Dadmun, M.; Zawodzinski, T. A.; Baker, G. A.; Tuckerman, M. E.; Savinell, R. F.; Sangoro, J. R. Deep Eutectic Solvents: A Review of Fundamentals and Applications. *Chem Rev* **2021**, *121* (3), 1232–1285. https://doi.org/10.1021/acs.chemrev.0c00385.

(45) Tabaraki, R.; Nazari, F. Microwave Synthesis of Carbon Dots in Ten Choline Chloride-Based Deep Eutectic Solvents: Effect of Solvent Molecular Structure on Carbon Dots Fluorescence and Sensing Properties. *J Photochem Photobiol A Chem* **2023**, *444*, 114891. https://doi.org/10.1016/j.jphotochem.2023.114891.

(46) Wang, Y.; Ma, C.; Liu, C.; Lu, X.; Feng, X.; Ji, X. Thermodynamic Study of Choline Chloride-Based Deep Eutectic Solvents with Water and Methanol. *J Chem Eng Data* **2020**, *65* (5), 2446–2457. https://doi.org/10.1021/acs.jced.9b01113.

(47) Hizaddin, H. F.; Hadj-Kali, M. K.; Ramalingam, A.; Ali Hashim, M. Extractive Denitrogenation of Diesel Fuel Using Ammonium- and Phosphonium-Based Deep Eutectic Solvents. *J Chem Thermodyn* **2016**, *95*, 164–173. https://doi.org/10.1016/j.jct.2015.12.009.

(48) Liu, Y.; Cao, Z.; Zhou, Z.; Zhou, A. Imidazolium-Based Deep Eutectic Solvents as Multifunctional Catalysts for Multisite Synergistic Activation of Epoxides and Ambient Synthesis of Cyclic Carbonates. *Journal of CO2 Utilization* **2021**, *53*, 101717. https://doi.org/10.1016/j.jcou.2021.101717.

(49) Sunol, A. K.; Sunol, S. G.; Cogswell, K.; Rooney, D.; Jacquemin, J.; García-álvarez, J.; Villanueva-Bermejo, D.; Fornari, T. Substitution Of Solvents By Safer Products. In *Handbook of Solvents, Volume 2: Use, Health, and Environment*; Elsevier, 2019; pp 1455–1634. https://doi.org/10.1016/B978-1-927885-41-3.50010-3.

(50) Florindo, C.; Oliveira, F. S.; Rebelo, L. P. N.; Fernandes, A. M.; Marrucho, I. M. Insights into the Synthesis and Properties of Deep Eutectic Solvents Based on Cholinium Chloride and Carboxylic Acids. *ACS Sustain Chem Eng* **2014**, *2* (10), 2416–2425. https://doi.org/10.1021/sc500439w.

(51) Sohal, N.; Basu, S.; Maity, B. Deciphering the Mechanism of Undoped and Heteroatom Doped-Carbon Dots for Detection of Lead Ions at Nanomolar Level. *Microchemical Journal* **2023**, *185*. https://doi.org/10.1016/j.microc.2022.108287.

(52) Liu, S.; Quan, T.; Yang, L.; Deng, L.; Kang, X.; Gao, M.; Xia, Z.; Li, X. *Supporting Information N,Cl-Co-Doped Carbon Dots from Impatiens Balsamina L. Stems and Deep Eutectic Solvent and Its Applications for Gram-Positive Bacteria Identification, Antibacterial, Cell Imaging and ClO-Sensing*.

(53) Pajewska-Szmyt, M.; Buszewski, B.; Gadzała-Kopciuch, R. Sulphur and Nitrogen Doped Carbon Dots Synthesis by Microwave Assisted Method as Quantitative Analytical Nano-Tool for Mercury Ion Sensing. *Mater Chem Phys* **2020**, *242*, 122484. https://doi.org/10.1016/j.matchemphys.2019.122484.

(54) Wang, Y.; Feng, M.; He, B.; Chen, X.; Zeng, J.; Sun, J. Ionothermal Synthesis of Carbon Dots from Cellulose in Deep Eutectic Solvent: A Sensitive Probe for Detecting Cu2+ and Glutathione with “off-on” Pattern. *Appl Surf Sci* **2022**, *599*. https://doi.org/10.1016/j.apsusc.2022.153705.

(55) Yin, Q.; Wang, M.; Fang, D.; Zhu, Y.; Yang, L. Novel N,Cl-Doped Deep Eutectic Solvents-Based Carbon Dots as a Selective Fluorescent Probe for Determination of Morphine in Food. *RSC Adv* **2021**, *11* (27), 16805–16813. https://doi.org/10.1039/d1ra00886b.

(56) Tabaraki, R.; Nazari, F. Fluorescent Nanoprobe for Detection of Naproxen Based on Doped Carbon Dots Prepared in Choline Chloride-Thiourea Deep Eutectic Solvent. *Journal of the Iranian Chemical Society* **2023**, *20* (5), 1031–1038. https://doi.org/10.1007/s13738-022-02702-9.

(57) Huang, Z. Y.; Wu, W. Z.; Li, Z. X.; Wu, Y.; Wu, C. B.; Gao, J.; Guo, J.; Chen, Y.; Hu, Y.; Huang, C. Solvothermal Production of Tea Residue Derived Carbon Dots by the Pretreatment of Choline Chloride/Urea and Its Application for Cadmium Detection. *Ind Crops Prod* **2022**, *184*. https://doi.org/10.1016/j.indcrop.2022.115085.

(58) Sachdev, A.; Gopinath, P. Green Synthesis of Multifunctional Carbon Dots from Coriander Leaves and Their Potential Application as Antioxidants, Sensors and Bioimaging Agents. *Analyst* **2015**, *140* (12), 4260–4269. https://doi.org/10.1039/c5an00454c.

(59) Ma, X.; Dong, Y.; Sun, H.; Chen, N. Highly Fluorescent Carbon Dots from Peanut Shells as Potential Probes for Copper Ion: The Optimization and Analysis of the Synthetic Process. *Mater Today Chem* **2017**, *5*, 1–10. https://doi.org/10.1016/j.mtchem.2017.04.004.

(60) Tyagi, A.; Tripathi, K. M.; Singh, N.; Choudhary, S.; Gupta, R. K. Green Synthesis of Carbon Quantum Dots from Lemon Peel Waste: Applications in Sensing and Photocatalysis. *RSC Adv* **2016**, *6* (76), 72423–72432. https://doi.org/10.1039/C6RA10488F.

(61) Kumar, A.; Chowdhuri, A. R.; Laha, D.; Mahto, T. K.; Karmakar, P.; Sahu, S. K. Green Synthesis of Carbon Dots from Ocimum Sanctum for Effective Fluorescent Sensing of Pb2+ Ions and Live Cell Imaging. *Sens Actuators B Chem* **2017**, *242*, 679–686. https://doi.org/10.1016/j.snb.2016.11.109.

(62) Miao, H.; Wang, Y.; Yang, X. Carbon Dots Derived from Tobacco for Visually Distinguishing and Detecting Three Kinds of Tetracyclines. *Nanoscale* **2018**, *10* (17), 8139–8145. https://doi.org/10.1039/C8NR02405G.

(63) Guo, Y.; Yang, L.; Li, W.; Wang, X.; Shang, Y.; Li, B. Carbon Dots Doped with Nitrogen and Sulfur and Loaded with Copper(II) as a "Turn-on" Fluorescent Probe for Cystein, Glutathione and Homocysteine. *Microchimica Acta* **2016**, *183* (4), 1409–1416. https://doi.org/10.1007/s00604-016-1779-6.

(64) Purbia, R.; Paria, S. A Simple Turn on Fluorescent Sensor for the Selective Detection of Thiamine Using Coconut Water Derived Luminescent Carbon Dots. *Biosens Bioelectron* **2016**, *79*, 467–475. https://doi.org/10.1016/j.bios.2015.12.087.

(65) Hu, Y.; Gao, Z. Sewage Sludge in Microwave Oven: A Sustainable Synthetic Approach toward Carbon Dots for Fluorescent Sensing of Para-Nitrophenol. *J Hazard Mater* **2020**, *382*, 121048. https://doi.org/10.1016/j.jhazmat.2019.121048.

(66) Raji, K.; Ramanan, V.; Ramamurthy, P. Facile and Green Synthesis of Highly Fluorescent Nitrogen-Doped Carbon Dots from Jackfruit Seeds and Its Applications towards the Fluorimetric Detection of Au^{3+} Ions in Aqueous Medium and in *in Vitro* Multicolor Cell Imaging. *New Journal of Chemistry* **2019**, *43* (29), 11710–11719. https://doi.org/10.1039/C9NJ02590A.

(67) Ensafi, A. A.; Hghighat Sefat, S.; Kazemifard, N.; Rezaei, B.; Moradi, F. A Novel One-Step and Green Synthesis of Highly Fluorescent Carbon Dots from Saffron for Cell Imaging and Sensing of Prilocaine. *Sens Actuators B Chem* **2017**, *253*, 451–460. https://doi.org/10.1016/j.snb.2017.06.163.

(68) Wang, L.; Bi, Y.; Hou, J.; Li, H.; Xu, Y.; Wang, B.; Ding, H.; Ding, L. Facile, Green and Clean One-Step Synthesis of Carbon Dots from Wool: Application as a Sensor for Glyphosate Detection Based on the Inner Filter Effect. *Talanta* **2016**, *160*, 268–275. https://doi.org/10.1016/j.talanta.2016.07.020.

(69) Wang, M.; Kang, X.; Deng, L.; Wang, M.; Xia, Z.; Gao, D. Deep Eutectic Solvent Assisted Synthesis of Carbon Dots Using Sophora Flavescens Aiton Modified with Polyethyleneimine:

Application in Myricetin Sensing and Cell Imaging. *Food Chem* **2021**, *345*, 128817. https://doi.org/10.1016/j.foodchem.2020.128817.

(70) Guo, Z.; Zheng, H.-Y.; Huang, Z.-Y.; Liu, Y.-Z.; Liu, Y.-H.; Chen, Y.; Gao, J.; Hu, Y.; Huang, C. Solvothermal Synthesis of Bifunctional Carbon Dots for Tartrazine and Fe(III) Detection from Chamomile Residue by Ternary DES Pretreatment. *Food Chem* **2023**, *426*, 136604. https://doi.org/10.1016/j.foodchem.2023.136604.

(71) Wang, Y.; Feng, M.; He, B.; Chen, X.; Zeng, J.; Sun, J. Ionothermal Synthesis of Carbon Dots from Cellulose in Deep Eutectic Solvent: A Sensitive Probe for Detecting Cu2+ and Glutathione with "off-on" Pattern. *Appl Surf Sci* **2022**, *599*, 153705. https://doi.org/10.1016/j.apsusc.2022.153705.

(72) Tabaraki, R.; Nazari, F. Comparison of Carbon Dots Prepared in Deep Eutectic Solvent and Water/Deep Eutectic Solvent: Study of Fluorescent Detection of Fe3+ and Cetirizine and Their Photocatalytic Antibacterial Activity. *J Fluoresc* **2022**, *32* (2), 549–558. https://doi.org/10.1007/s10895-021-02875-1.

(73) Shaabani, A.; Hooshmand, S. E. Choline Chloride/Urea as a Deep Eutectic Solvent/Organocatalyst Promoted Three-Component Synthesis of 3-Aminoimidazo-Fused Heterocycles via Groebke-Blackburn-Bienayme Process. *Tetrahedron Lett* **2016**, *57* (3), 310–313. https://doi.org/10.1016/j.tetlet.2015.12.014.

(74) Crosby, G. A.; Demas, J. N. Measurement of Photoluminescence Quantum Yields. Review. *J Phys Chem* **1971**, *75* (8), 991–1024. https://doi.org/10.1021/j100678a001.

(75) Bajpai, S. K.; D'Souza, A.; Suhail, B. Blue Light-Emitting Carbon Dots (CDs) from a Milk Protein and Their Interaction with Spinacia Oleracea Leaf Cells. *Int Nano Lett* **2019**, *9* (3), 203–212. https://doi.org/10.1007/s40089-019-0271-9.

(76) Siddique, A. B.; Pramanick, A. K.; Chatterjee, S.; Ray, M. Amorphous Carbon Dots and Their Remarkable Ability to Detect 2,4,6-Trinitrophenol. *Sci Rep* **2018**, *8* (1), 9770. https://doi.org/10.1038/s41598-018-28021-9.

(77) Gao, Z.; Li, X.; Shi, L.; Yang, Y. Deep Eutectic Solvents-Derived Carbon Dots for Detection of Mercury (II), Photocatalytic Antifungal Activity and Fluorescent Labeling for C. Albicans. *Spectrochim Acta A Mol Biomol Spectrosc* **2019**, *220*, 117080. https://doi.org/10.1016/j.saa.2019.04.072.

(78) Boonmee, C.; Promarak, V.; Tuntulani, T.; Ngeontae, W. Cysteamine-Capped Copper Nanoclusters as a Highly Selective Turn-on Fluorescent Assay for the Detection of Aluminum Ions. *Talanta* **2018**, *178*, 796–804. https://doi.org/10.1016/j.talanta.2017.10.006.

(79) Yin, Q.; Wang, M.; Fang, D.; Zhu, Y.; Yang, L. Novel N,Cl-Doped Deep Eutectic Solvents-Based Carbon Dots as a Selective Fluorescent Probe for Determination of Morphine in Food. *RSC Adv* **2021**, *11* (27), 16805–16813. https://doi.org/10.1039/D1RA00886B.

(80) Yang, L.; Jiang, W.; Qiu, L.; Jiang, X.; Zuo, D.; Wang, D.; Yang, L. One Pot Synthesis of Highly Luminescent Polyethylene Glycol Anchored Carbon Dots Functionalized with a Nuclear Localization Signal Peptide for Cell Nucleus Imaging. *Nanoscale* **2015**, *7* (14), 6104–6113. https://doi.org/10.1039/C5NR01080B.

(81) Hu, S.; Chang, Q.; Lin, K.; Yang, J. Tailoring Surface Charge Distribution of Carbon Dots through Heteroatoms for Enhanced Visible-Light Photocatalytic Activity. *Carbon N Y* **2016**, *105*, 484–489. https://doi.org/10.1016/j.carbon.2016.04.078.

(82) Çalhan, S. D.; Alaş, M. Ö.; Aşık, M.; Kaya, F. N. D.; Genç, R. One-Pot Synthesis of Hydrophilic and Hydrophobic Fluorescent Carbon Dots Using Deep Eutectic Solvents as Designer Reaction Media. *J Mater Sci* **2018**, *53* (22), 15362–15375. https://doi.org/10.1007/s10853-018-2723-4.

(83) Reckmeier, C. J.; Schneider, J.; Susha, A. S.; Rogach, A. L. Luminescent Colloidal Carbon Dots: Optical Properties and Effects of Doping [Invited]. *Opt Express* **2016**, *24* (2), A312. https://doi.org/10.1364/OE.24.00A312.

(84) Chandra, S.; Bano, D.; Pradhan, P.; Singh, V. K.; Yadav, P. K.; Sinha, D.; Hasan, S. H. Nitrogen/Sulfur-Co-Doped Carbon Quantum Dots: A Biocompatible Material for the Selective Detection of Picric Acid in Aqueous Solution and Living Cells. *Anal Bioanal Chem* **2020**, *412* (15), 3753–3763. https://doi.org/10.1007/s00216-020-02629-1.

(85) Yan, F.; Zou, Y.; Wang, M.; Mu, X.; Yang, N.; Chen, L. Highly Photoluminescent Carbon Dots-Based Fluorescent Chemosensors for Sensitive and Selective Detection of Mercury Ions and Application of Imaging in Living Cells. *Sens Actuators B Chem* **2014**, *192*, 488–495. https://doi.org/10.1016/j.snb.2013.11.041.

(86) Pajewska-Szmyt, M.; Buszewski, B.; Gadzała-Kopciuch, R. Carbon Dots as Rapid Assays for Detection of Mercury(II) Ions Based on Turn-off Mode and Breast Milk. *Spectrochim Acta A Mol Biomol Spectrosc* **2020**, *236*. https://doi.org/10.1016/j.saa.2020.118320.

(87) Ren, G.; Meng, Y.; Zhang, Q.; Tang, M.; Zhu, B.; Chai, F.; Wang, C.; Su, Z. Nitrogen-Doped Carbon Dots for the Detection of Mercury Ions in Living Cells and Visualization of Latent Fingerprints. *New Journal of Chemistry* **2018**, *42* (9), 6824–6830. https://doi.org/10.1039/c7nj05170k.

(88) Li, L.; Yu, B.; You, T. Nitrogen and Sulfur Co-Doped Carbon Dots for Highly Selective and Sensitive Detection of Hg (II) Ions. *Biosens Bioelectron* **2015**, *74*, 263–269. https://doi.org/10.1016/j.bios.2015.06.050.

(89) Zhang, R.; Chen, W. Nitrogen-Doped Carbon Quantum Dots: Facile Synthesis and Application as a "Turn-off" Fluorescent Probe for Detection of Hg2+ Ions. *Biosens Bioelectron* **2014**, *55*, 83–90. https://doi.org/10.1016/j.bios.2013.11.074.

(90) Xie, Y.; Cheng, D.; Liu, X.; Han, A. Green Hydrothermal Synthesis of N-Doped Carbon Dots from Biomass Highland Barley for the Detection of Hg2+. *Sensors (Switzerland)* **2019**, *19* (14). https://doi.org/10.3390/s19143169.

(91) Karami, C.; Taher, M. A.; Shahlaei, M. A Simple Method for Determination of Mercury (II) Ions by PNBS-Doped Carbon Dots as a Fluorescent Probe. *Journal of Materials Science: Materials in Electronics*. Springer April 1, 2020, pp 5975–5983. https://doi.org/10.1007/s10854-020-03157-5.

(92) Singh, V. K.; Singh, V.; Yadav, P. K.; Chandra, S.; Bano, D.; Koch, B.; Talat, M.; Hasan, S. H. Nitrogen Doped Fluorescent Carbon Quantum Dots for on-off-on Detection of Hg2+ and Glutathione in Aqueous Medium: Live Cell Imaging and IMPLICATION Logic Gate Operation. *J Photochem Photobiol A Chem* **2019**, *384*, 112042. https://doi.org/10.1016/j.jphotochem.2019.112042.

(93) Zhang, M.; Wang, W.; Yuan, P.; Chi, C.; Zhang, J.; Zhou, N. Synthesis of Lanthanum Doped Carbon Dots for Detection of Mercury Ion, Multi-Color Imaging of Cells and Tissue, and Bacteriostasis. *Chemical Engineering Journal* **2017**, *330*, 1137–1147. https://doi.org/10.1016/j.cej.2017.07.166.

(94) Wang, P.; Yan, Y.; Zhang, Y.; Gao, T.; Ji, H.; Guo, S.; Wang, K.; Xing, J.; Dong, Y. An Improved Synthesis of Water-Soluble Dual Fluorescence Emission Carbon Dots from Holly Leaves for Accurate Detection of Mercury Ions in Living Cells. *Int J Nanomedicine* **2021**, *Volume 16*, 2045–2058. https://doi.org/10.2147/IJN.S298152.

(95) Pang, L. F.; Wu, H.; Fu, M. J.; Guo, X. F.; Wang, H. Red Emissive Boron and Nitrogen Co-Doped "on-off-on" Carbon Dots for Detecting and Imaging of Mercury(II) and Biothiols. *Microchimica Acta* **2019**, *186* (11). https://doi.org/10.1007/s00604-019-3852-4.

(96) Cai, L.; Fu, Z.; Cui, F. Synthesis of Carbon Dots and Their Application as Turn Off–On Fluorescent Sensor for Mercury (II) and Glutathione. *J Fluoresc* **2020**, *30* (1), 11–20. https://doi.org/10.1007/s10895-019-02454-5.

(97) Wang, Y.; Feng, M.; He, B.; Chen, X.; Zeng, J.; Sun, J. Ionothermal Synthesis of Carbon Dots from Cellulose in Deep Eutectic Solvent: A Sensitive Probe for Detecting Cu2+ and Glutathione with "off-on" Pattern. *Appl Surf Sci* **2022**, *599*, 153705. https://doi.org/10.1016/j.apsusc.2022.153705.

(98) Cai, Q. Y.; Li, J.; Ge, J.; Zhang, L.; Hu, Y. L.; Li, Z. H.; Qu, L. B. A Rapid Fluorescence "Switch-on" Assay for Glutathione Detection by Using Carbon Dots-MnO2 Nanocomposites. *Biosens Bioelectron* **2015**, *72*, 31–36. https://doi.org/10.1016/j.bios.2015.04.077.

(99) Gu, J.; Hu, D.; Wang, W.; Zhang, Q.; Meng, Z.; Jia, X.; Xi, K. Carbon Dot Cluster as an Efficient "off-on" Fluorescent Probe to Detect Au(III) and Glutathione. *Biosens Bioelectron* **2015**, *68*, 27–33. https://doi.org/10.1016/j.bios.2014.12.027.

(100) Liang, Y.; Xu, L.; Tang, K.; Guan, Y.; Wang, T.; Wang, H.; Yu, W. W. Nitrogen-Doped Carbon Dots Used as an "on–off–on" Fluorescent Sensor for Fe3+ and Glutathione Detection. *Dyes and Pigments* **2020**, *178*. https://doi.org/10.1016/j.dyepig.2020.108358.

(101) Singh, V. K.; Singh, V.; Yadav, P. K.; Chandra, S.; Bano, D.; Koch, B.; Talat, M.; Hasan, S. H. Nitrogen Doped Fluorescent Carbon Quantum Dots for On-off-on Detection of Hg2+ and Glutathione in Aqueous Medium: Live Cell Imaging and IMPLICATION Logic Gate Operation. *J Photochem Photobiol A Chem* **2019**, *384*. https://doi.org/10.1016/j.jphotochem.2019.112042.

(102) Liu, A.; Cai, H.; Xu, Z.; Li, J.; Weng, X.; Liao, C.; He, J.; Liu, L.; Wang, Y.; Qu, J.; Li, H.; Song, J.; Guo, J. Multifunctional Carbon Dots for Glutathione Detection and Golgi Imaging. *Talanta* **2023**, *259*, 124520. https://doi.org/10.1016/j.talanta.2023.124520.

(103) Pan, J.; Zheng, Z.; Yang, J.; Wu, Y.; Lu, F.; Chen, Y.; Gao, W. A Novel and Sensitive Fluorescence Sensor for Glutathione Detection by Controlling the Surface Passivation Degree of Carbon Quantum Dots. *Talanta*. Elsevier B.V. May 1, 2017, pp 1–7. https://doi.org/10.1016/j.talanta.2017.01.033.

(104) Liang, C.; Xie, X.; Zhang, D.; Feng, J.; Lu, S.; Shi, Q. Biomass Carbon Dots Derived from *Wedelia Trilobata* for the Direct Detection of Glutathione and Their Imaging Application in Living Cells. *J Mater Chem B* **2021**, *9* (28), 5670–5681. https://doi.org/10.1039/D0TB02979C.

(105) Sohal, N.; Bhatia, S. K.; Basu, S.; Maity, B. Nanomolar Level Detection of Metal Ions by Improving the Monodispersity and Stability of Nitrogen-Doped Graphene Quantum Dots. *New Journal of Chemistry* **2021**, *45* (42), 19941–19949. https://doi.org/10.1039/D1NJ04551B.

(106) Zu, F.; Yan, F.; Bai, Z.; Xu, J.; Wang, Y.; Huang, Y.; Zhou, X. The Quenching of the Fluorescence of Carbon Dots: A Review on Mechanisms and Applications. *Microchimica Acta* **2017**, *184* (7), 1899–1914. https://doi.org/10.1007/s00604-017-2318-9.

(107) Sohal, N.; Maity, B.; Basu, S. Recent Advances in Heteroatom-Doped Graphene Quantum Dots for Sensing Applications. *RSC Adv* **2021**, *11* (41), 25586–25615. https://doi.org/10.1039/D1RA04248C.

(108) Zu, F.; Yan, F.; Bai, Z.; Xu, J.; Wang, Y.; Huang, Y.; Zhou, X. The Quenching of the Fluorescence of Carbon Dots: A Review on Mechanisms and Applications. *Microchimica Acta* **2017**, *184* (7), 1899–1914. https://doi.org/10.1007/s00604-017-2318-9.

(109) Ji, W.; Yu, J.; Cheng, J.; Fu, L.; Zhang, Z.; Li, B.; Chen, L.; Wang, X. Dual-Emissive Near-Infrared Carbon Dot-Based Ratiometric Fluorescence Sensor for Lysozyme. *ACS Appl Nano Mater* **2022**, *5* (1), 1656–1663. https://doi.org/10.1021/acsanm.1c04435.

(110) Wei, J.; Yuan, Y.; Li, H.; Hao, D.; Sun, C.; Zheng, G.; Wang, R. A Novel Fluorescent Sensor for Water in Organic Solvents Based on Dynamic Quenching of Carbon Quantum Dots. *New Journal of Chemistry* **2018**, *42* (23), 18787–18793. https://doi.org/10.1039/C8NJ04365E.

(111) Luo, D.; Liu, S. G.; Li, N. B.; Luo, H. Q. Water-Soluble Polymer Dots Formed from Polyethylenimine and Glutathione as a Fluorescent Probe for Mercury(II). *Microchimica Acta* **2018**, *185* (6), 284. https://doi.org/10.1007/s00604-018-2817-3.

(112) Yan, F.; Bai, Z.; Zu, F.; Zhang, Y.; Sun, X.; Ma, T.; Chen, L. Yellow-Emissive Carbon Dots with a Large Stokes Shift Are Viable Fluorescent Probes for Detection and Cellular Imaging of Silver Ions and Glutathione. *Microchimica Acta* **2019**, *186* (2), 113. https://doi.org/10.1007/s00604-018-3221-8.

(113) Chen, S.; Hao, Y.; Li, R.; Liu, Y.; Li, J.; Geng, L. N-Doped Carbon Dots as the Multifunctional Fluorescent Probe for Mercury Ion, Glutathione and PH Detection. *Nanotechnology* **2023**, *34* (12). https://doi.org/10.1088/1361-6528/acade7.

(114) Zu, F.; Yan, F.; Bai, Z.; Xu, J.; Wang, Y.; Huang, Y.; Zhou, X. The Quenching of the Fluorescence of Carbon Dots: A Review on Mechanisms and Applications. *Microchimica Acta* **2017**, *184* (7), 1899–1914. https://doi.org/10.1007/s00604-017-2318-9.

(115) Sohal, N.; Maity, B.; Basu, S. Morphology-Dependent Performance of MnO_2 Nanostructure–Carbon Dot-Based Biosensors for the Detection of Glutathione. *ACS Appl Bio Mater* **2021**, *4* (6), 5158–5168. https://doi.org/10.1021/acsabm.1c00353.

M.Sc Dissertation Plag Check

ORIGINALITY REPORT

14%	7%	12%	1%
SIMILARITY INDEX	INTERNET SOURCES	PUBLICATIONS	STUDENT PAPERS

PRIMARY SOURCES

1	www.mdpi.com Internet Source	1%
2	Shaochi Liu, Tian Quan, Lijuan Yang, Linlin Deng, Xun Kang, Manjie Gao, Zhining Xia, Xiang Li, Die Gao. " N,Cl-Codoped Carbon Dots from L. Stems and a Deep Eutectic Solvent and Their Applications for Gram-Positive Bacteria Identification, Antibacterial Activity, Cell Imaging, and ClO Sensing ", ACS Omega, 2021 Publication	1%
3	Yin Zhong, Qi Chen, Junjian Li, Xihao Pan, Zhiwei Han, Wei Dong. "One-Step Synthesis of Nitrogen and Chlorine Co-Doped Carbon Quantum Dots for Detection of Fe3+", Nano, 2017 Publication	1%

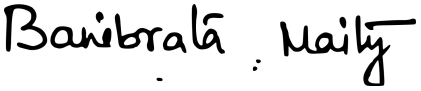

Exclude quotes	Off	Exclude matches	Off
Exclude bibliography	Off		